THESIS FOR THE DEGREE OF DOCTOR OF PHILOSOPHY

CONCATEMERIZATION OF SYNTHETIC OLIGONUCLEOTIDES

ASSEMBLY AND LIGAND INTERACTIONS

LU SUN

Department of Chemical and Biological Engineering
CHALMERS UNIVERSITY OF TECHNOLOGY
GÖTEBORG, SWEDEN 2014

Concatemerization of Synthetic Oligonucleotides

Assembly and Ligand Interactions

LU SUN

ISBN 978-91-7597-092-9

Doktorsavhandlingar vid Chalmers tekniska högskola

Ny serie nr 3773

ISSN 0346-718X

Department of Chemical and Biological Engineering

Chalmers University of Technology

SE-412 96 Göteborg

Sweden

Telephone + 46 (0)31-772 1000

Cover image:

Two ways of forming DNA concatemers. (Top right) Self-assembly of oligonucleotides in free solution. (Down) A three-step sequential assembly of DNA concatemer layer on a planar surface and RAD51 induced DNA layer extension.

Back cover photo: © Keling Bi

Printed by Chalmers Reproservice

Göteborg, Sweden 2014

Concatemerization of Synthetic Oligonucleotides Assembly and Ligand Interactions

LU SUN
Department of Chemical and Biological Engineering
Chalmers University of Technology

ABSTRACT
DNA nanotechnology has become an important research field because of its advantages in high predictability and accuracy of base paring recognition. For example, the DNA concatemer, one of the simplest DNA constructs in shape, has been used to enhance signals in biosensing. In this thesis, concatemers were designed and characterized towards sequence-specific target amplifiers for single-molecule mechanical studies.

The project firstly focuses on exploring how to obtain concatemers of satisfactory length by self-assembly in bulk. Concatemers formed in solution by mixing of the different components are characterized using gel electrophoresis and AFM. Experimental results demonstrate that the concatemerization yield could be increased primarily by increasing the ionic strength, and linear concatemers of expected length could be separated from mixed sizes and shapes. As an alternative, a platform for concatemer formation based on a planar surface is investigated by immobilizing and sequentially hybridizing oligonucleotides to concatemers. This method has been further improved by involving click reaction to seal the nicks on the DNA backbone. The sequential construction process is monitored using QCM-D and SPR, and formed DNA constructs are determined using gel electrophoresis which confirms that concatemers of desired lengths are successfully formed in a controllable manner.

Furthermore, QCM-D and SPR are also applied to study DNA-ligand interaction on the surface-based concatemer formation platform. We select three ligands, known to bind to DNA: spermidine, spermine, and RAD51. It is observed that polyamines condense the DNA layers; by contrast, RAD51 induces an extension of the DNA layer. This study provides some guidelines for QCM-D and SPR-based characterization of changes in the properties of DNA films (e.g., thickness and viscoelastic properties) on sensor surfaces. It is interesting to correlate these structural and mechanical changes induced in single DNA molecules upon ligand binding. The biosensing approach provides rapid access to kinetic data of DNA-ligand interactions, which is typically useful in various screening applications.

Keywords: DNA concatemer, DNA formation, self-assembly, hybridization, DNA-binding, gel electrophoresis, QCM-D

LIST OF PUBLICATIONS

This thesis is based on the work contained in the following papers, referred to by Roman numerals in the text:

Paper I:

Characterization of Self-Assembled DNA Concatemers From Synthetic Oligonucleotides

Lu Sun, Björn Åkerman*

Computational and Structural Biotechnology Journal, **2014**, 11 (18), 66-72

Paper II:

Platform for Assembly, Click Chemistry Modification and Release of DNA Concatemers on a Planar Surface Studied By QCM-D and Gel Electrophoresis

Lu Sun*, Sofia Svedhem, Afaf, H. El-Sagheer, Tom Brown, Björn Åkerman

Manuscript

Paper III:

Construction and Modelling of Concatemeric DNA Multilayers on a Planar Surface as Monitored by QCM-D and SPR

Lu Sun, Sofia Svedhem, Björn Åkerman*

Langmuir, **2014**, 30 (28), 8432-8441

Paper IV:

Sensing Conformational Changes in DNA upon Ligand Binding Using QCM-D. Polyamine Condensation and Rad51 Extension of DNA Layers

Lu Sun, Karolin Frykholm, Louise H. Fornander, Sofia Svedhem, Fredrik Westerlund, Björn Åkerman*

Journal of Physical Chemistry B,**2014**, 118 (41), 11895-11904

CONTRIBUTION REPORT

Paper I

Designed and performed the experiments, analysed the results, and wrote the paper.

Paper II

Designed and performed the experiments, analysed the results, and wrote the paper.

Paper III

Designed and performed the experiments, analysed the results, performed all modelling calculations, and wrote the paper.

Paper IV

Designed most, and performed all the experiments, analysed the results, and wrote the paper.

Table of Contents

CHAPTER 1

INTRODUCTION

Deoxyribonucleic acid (DNA), the hereditary material in most organisms on earth, is a molecule that has fascinated the world ever since its discovery in 1869.[1] But it took almost a century, for scientists to understand its structure, biological significance to cell function, and to proove that it is responsible for inherited traits. The well-known structure of DNA, the double helix, proposed by James Watson and Francis Crick in 1953,[2] has been used as an icon of popular science for decades. The research work on discovery of the structural properties and biological function of DNA still leads investigations in diverse areas. For example, the largest collaborative biological project in the world to date, the Human Genome project, managed to assemble and interpret the base sequence of human DNA, which continues to provide avenues for advances in medicine and biotechnology.[3] One of the substantial innovative research is to utilize DNA strand as a building block in fabrication of nanoconstructs and related devices due to its inherent physical properties, i.e., nanoscale dimension, predictable assembly, and high structural stability and stiffness.[4] During the past decades, research work involving DNA has been extensively carried out and has achieved remarkable progress in an interdisciplinary field that connects chemistry, physics, biology, pharmaceutics, material science, nanotechnology, etc.

1.1 Motivation

DNA underpins all processes that take place within a cell; investigations on DNA interacting with proteins or small molecules (ligands) are therefore of great importance in understanding the fundamental processes of life. In order to have a thorough understanding of DNA-ligand/protein interaction, investigations require new techniques that are capable of studying mechanical properties of DNA during interactions in detail.

Optical tweezers as one of the most developed single-molecule detection (SMD) techniques, have had great success in uncovering fundamentals of the mechanical properties of biosystems, such as stretching DNA[5-9] and DNA-protein interactions.[10,11] However, the investigated DNA molecules are mostly chromosomal DNA containing base sequences in an order given by the biological function, until Bosaeus *et al*[8] reported

on stretching of sequence-designed DNA. Automation of DNA synthesis has achieved great development regarding synthesis of the sequence of DNA at will,[12] but a crucial and practical limit is not easy to overcome that is that the length of synthetic oligonucleotide cannot reach over 200 base pairs (bp).[13] That is why the investigations on designed sequences of DNA stretching were only on molecules of 60-122 bp long.[8,9]

The DNA concatemer, sometimes spelt as concatamer, is a linear long polymer structure assembled by short DNA fragments via specific interactions.[14] The first description of DNA concatemerization dates back to 1980.[15] It is noticed that the efficiency of the reported concatemerization was significantly lowered by the by-process of hairpin formation. To obviate this slow process, two different oligonucleotides with mutually complementary sequences can be used to form duplex with sticky ends. In recent years, DNA concatemers have been employed as signal amplifiers for detection of cellular uptake of DNA,[16] virus DNA,[17] IgG,[18] ATP,[19] and copper (II)[20] with high sensitivity. Yet, concatemeric DNA molecules with designed sequences for studies of sequence-specific DNA-protein/ligand interactions have never been explored by SMD techniques. Guided by the interest of understanding how ligands and proteins interact with DNA molecules with specific sequences, concatemerization of predesigned synthetic oligonucleotides is investigated for studying the DNA-actinomycin D interactions at the single-molecule level using optical tweezers in the future.

1.2 Aim of the Thesis

A long term goal of this project is to apply concatemeric DNA molecules (about 500bp) to study single DNA molecule interacting with ligands using optical tweezers. With repetitive sequences, each concatemer provides additional possibilities for ligands to bind (Figure 1.1). Moreover, when DNA molecules are synthesized with bulky groups, such as the halogen group elements (Br, I) or methyl on the base residues,[21] major or minor groove binders can be distinguished if the obstruction of one or both grooves changed the binding constant. In addition, concatemers may also be long enough to orient in shear flow to study DNA interactions by linear dichroism spectroscopy, which is a well established spectroscopic method to study DNA-ligand interactions in bulk.[22]

This thesis focuses on the formation of linear DNA concatemers with well-defined and repetitive sequences, but also emphasizing the value of practical ways for forming concatemers. The starting point is to test whether self-assembly of presynthesized oligonucleotides in bulk solution is an efficient method. Sizes and shapes of formed concatemers are analysed using gel electrophoresis and AFM. Then, assembly of concatemers is explored on a surface-based method combined with the surface-sensitive techniques QCM-D and SPR. Since QCM-D and SPR have been used to study many

biomolecules, including DNA,[23-27] the formation of concatemers and the subsequent concatemers-ligand interactions are monitored using QCM-D and SPR presented here, point out the usefullness of these methods for sensing conformational changes of DNA during an interaction.

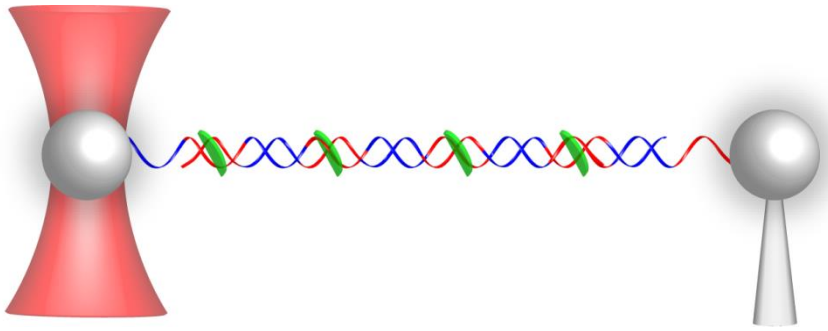

Figure 1.1 Schematic illustration of stretching experiment using assembled DNA concatemers to study single DNA molecule interacting with ligands using optical tweezers, where ligands (green ellipses) only bind to the repeated target sequence (in red) in the DNA concatemer.

1.3 Contents of the Thesis

Assembly of DNA concatemers is of special interests in this thesis. Due to the simplicity of the structure, DNA concatemers are considered as one-dimensional DNA constructs, which can be assembled via spontaneous base pairing recognition between predesigned oligonucleotides. Before discussing the results and conclusion, fundamental information regarding to this study is explained.

Chapter 2 introduces the basic concept and background of nucleic acids, including their discovery history, biological functions and structures, and DNA-ligand interactions. Some advanced structures of DNA nanoconstructs are also stated. Chapter 3 presents the concept of surface modification, introduces biomolecules involved in surface-based studies, and exhibits several examples of chemically modified DNA molecules. Chapter 4 describes experimental devices utilized in this study.

Chapter 5 summarizes the results of the performed experimental work. An overview of Chapter 5 is schematically illustrated in Figure 1.2. The first study concerns the formation of concatemers by self-assembly in bulk solution. Incubation conditions were optimized to obtain as long concatemers as possible (*Paper I*). However, a large portion of non-linear concatemers were also detected, which could probably be a result of circular formation of concatemers. To avoid these undesired structures, the second part of the thesis focuses on establishing a platform that can form only linear concatemers on a planar surface (*Paper II*). The platform has the advantage of yielding DNA duplexes of desired lengths and sequences at will. Improvement of this platform is further investigated

by involving click chemistry reactions to close the nicks on the backbone of concatemers (*Paper II*). Moreover, linear concatemers are trimmed off the surface (*Paper II*) for further studies. The platform is studied by QCM-D and SPR. It is investigated whether the Voigt-based modelling of the viscoelastic properties of a polymer film gives a comprehensive description of the experimental data (*Paper III*). With the knowledge of using a viscoelastic model to understand DNA layer, the possibility of applying the platform for investigating DNA-ligand/protein interactions for biosensing is also demonstrated in the thesis (*Paper IV*).

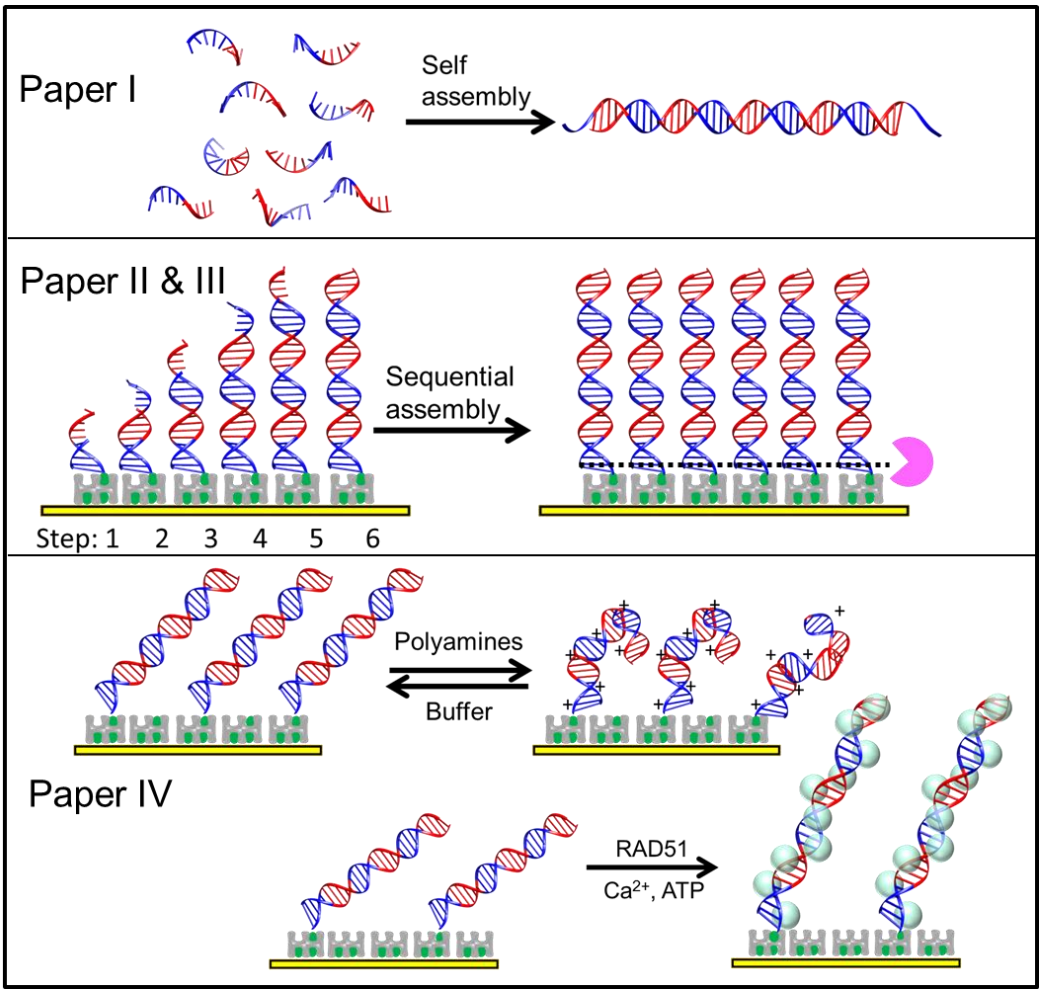

Figure 1.2 Overview of the topics covered in Papers I-IV. Paper I relates to self-assembly of DNA concatemers. Paper II and III develop a platform for forming DNA multilayers on a planar surface. Paper IV reports on sensing changes on structural properties in the DNA layer. These changes are correlated to conformational changes in DNA rationalizing the observed changes in film thickness.

Chapter 6 concludes the achievements with suggestions for future work.

CHAPTER 2

BACKGROUND OF NUCLEIC ACIDS

Nucleic acids are polymeric chains containing varying numbers of nucleotides as monomers. Each nucleotide is composed of three components: a sugar, a phosphate group and a heterocyclic base. The two types of nucleic acids are deoxyribonucleic acid (DNA) and ribonucleic acid (RNA), depending on if the sugar is a deoxyribose or a ribose. DNA carries the hereditary information, and RNA helps to convert genetic information from genes into certain amino acids sequence of proteins.

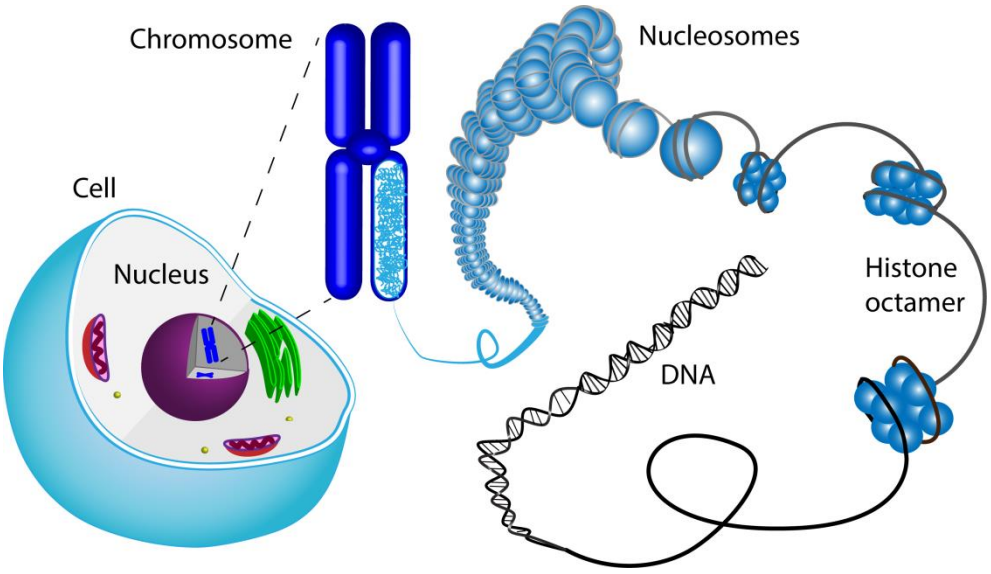

Figure 2.1 Illustration of the location and structure of DNA in an eukaryotic cell. DNA is stretched to demonstrate how it interacts with histones to form nucleosomes and chromosomes.

The timeline for the discovery of DNA stretches over 100 years. Friedrich Miescher first discovered DNA in 1869[28] and named it "nuclein" because it was found in the cell nucleus. Actually, nuclein is a very large DNA molecule that binds with many copies of several different proteins or other molecules in a highly compact structure called nucleosome nowadays. Nucleosomes are folded in highly compacted manner to form a chromosome, all of which locate in the nucleus of the cells (Figure 2.1). DNA can also be found in small amounts in mitochondria and chloroplasts. The total chromosomes of an organism is referred to as its chromosomal genome; and the DNA that constitutes it is

referred to as genomic DNA. The human genome is discovered with approximately 3.2 billion base pairs of DNA arranged into 46 chromosomes.[29]

2.1 Biological Roles of DNA

The biological function of DNA comprises both preservation and utilization of genetic information. The former is achieved through DNA self-replication, which are units of heredity that is transmitted from generation to generation; the latter is accomplished by means of the control of the synthesis of proteins through transcription and translation.[30]

Many decades following Mieschers' discovery, due to the complexity of proteins, most scientists believed that protein, rather than DNA, was the carrier of genetic information. This misinterpretation was not changed until 1944, when Oswald Avery and co-workers published their landmark work to highlight that DNA, not protein as previously believed, was the genetic material.[31] In 1952, Alfred Hershey and Martha Chase further confirmed that DNA is the only material transferred directly from bacteriophages to bacteria when the bacteria were infected by viruses.[32] With the discovery that DNA contains the genetic information, the key question turns to how this information was stored and replicated in DNA. The reason that DNA can perform all the biological functions is a direct consequence of the unique ability for proteins and other molecules to recognise specific DNA structural features.

2.2 DNA Structure

In the very beginning of isolating DNA, Miescher noticed that nuclein contained large amounts of phosphorous. Then Albrecht Kossel, discovered that nuclein, when broken down, contained carbohydrates and nitrogen-bearing compounds: two bicyclic purines, guanine (G) and adenine (A); and two monocyclic pyrimidines, thymine (T), and cytosine (C).[33,34] Phoebus Levene found that the carbohydrate in yeast nucleic acids was the pentose sugar ribose[35], and the carbohydrate in thymus nucleic acids was also a pentose sugar but lacks one oxygen atom of ribose, referred to as deoxyribose.[36] By the beginning of 20th century, DNA was known to contain building blocks of nucleotides which are composed of three components: a nitrogenous base, a pentose sugar (deoxyribose), and a phosphate group (Figure 2.2). In addition, the polynucleotide structure of DNA proposed by Levene[37] was well accepted. However, people did not figure out the exact or the three dimensional (3D) structure of the molecule.

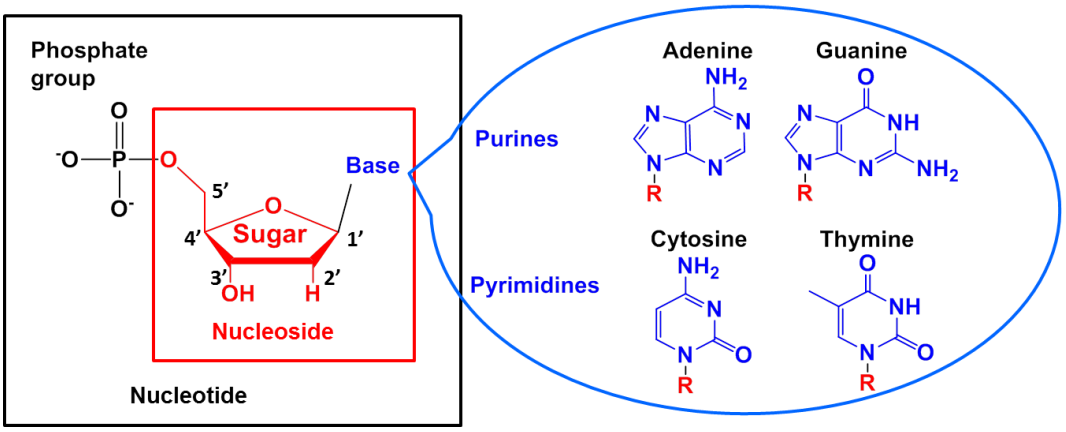

Figure 2.2 Chemical structure a nucleotide, which consists of a phosphate group, a pentose sugar, and one of the four bases (in blue): adenine (A), guanine (G), cytosine (C), or thymine (T). A molecule made of a nitrogenous base and deoxyribose sugar, is called a nucleoside (in red square). When a phosphate molecule is attached to the opposite side of the sugar, it forms a nucleotide (in black square).

By the early 1950s, at least two groups were in the race for discovering the structure of DNA, James Watson and Francis Crick in Cambridge University decided to go straight to build a DNA model, while Rosalind Franklin and Maurice Wilkins at King's College in London used X-ray to understand DNA. Franklin found that there were two forms of DNA, the dry form, A, and the wet form, B, both ended up in helix structure.[38] In the same year, by referring to Franklin's X-ray image, "Exposure 51", Watson and Crick deciphered a double helical model of B-form DNA.[39]

Watson and Crick's model has four major features, which are almost the same as we know the structure today. First, the two DNA strands form a helical spiral, intertwining around the same helix axis in a right-handed spiral (Figure 2.3a). Second, the sugar-phosphate backbones are on the outside of the helix, each sugar attaches one base which is perpendicular to the path of the backbone pointing inside of the helix (Figure 2.3b). Third, the two strands are connected by hydrogen bonds (Figure 2.3c) in a way that adenines bind to thymines via two hydrogen bonds, and cytosines bind to guanines via three hydrogen bonds, which is consistent with Chargaff's rule.[40] Last, the double strand is antiparallel, in which the two strands both point from the 5'-end to the 3'-end, but are aligned in opposite directions (Figure 2.3c).

In the year of 1953, Franklin and Wilkins' work appeared as supporting articles,[41,42] confirming Watson-Crick's model of B-form DNA by the X-ray diffraction data. They reported that the helix has a pitch of 34 Å (10 base pairs), the distance between two adjacent base residues is 3.4 Å, and the helix diameter is 20 Å (Figure 2.4 left). Under conditions of low humidity, DNA is favoured in another right-handed conformation, but

with a smaller helical pitch of 25 Å, a smaller distance between two adjacent base residues of 2.4 Å, and a bigger helix diameter of 23 Å, namely A-form DNA (Figure 2.4 middle). Both A- and B-form DNA have distinguishing grooves, the major groove and the minor groove.

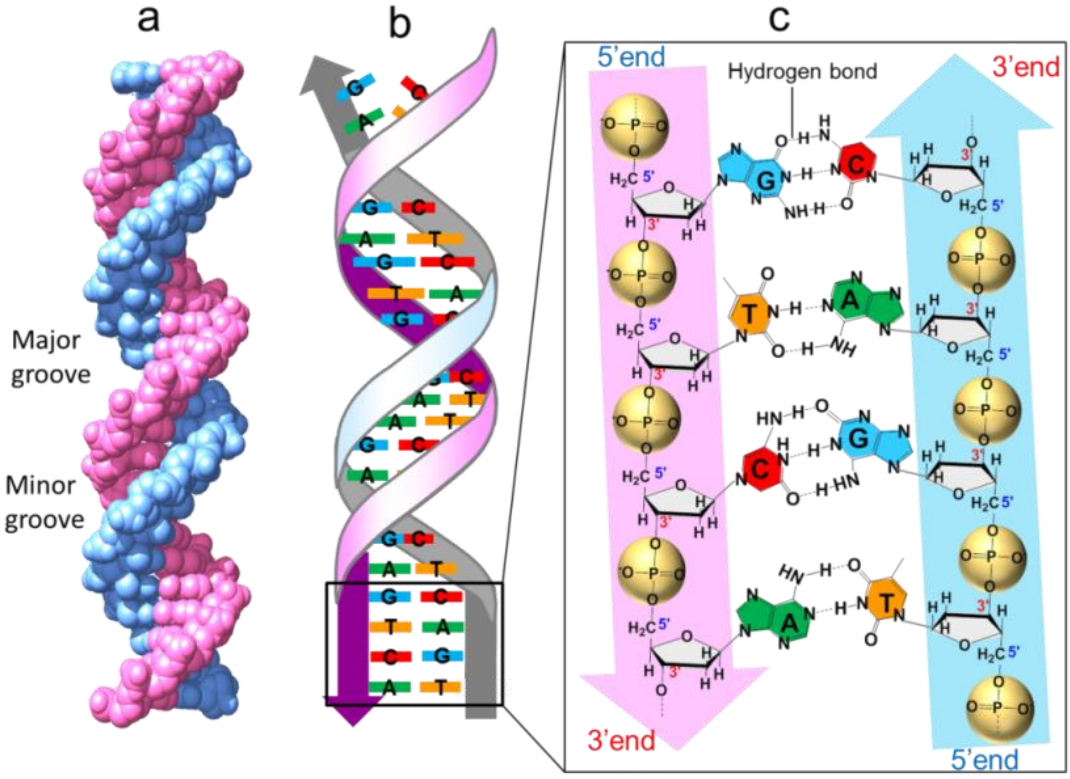

Figure 2.3 Illustration of the molecular structure of DNA. (a) Simplified illustration of two strands being winding around and forming a spiral helix. (b) Base pairing in DNA. (c) Detailed information of base pairing via hydrogen bonds and the 5' to 3' direction of two sugar-phosphate backbones.

A left-handed DNA was discovered and its helical structure was determined in 1970's.[43,44] It is named Z-DNA, due to the zig-zag course followed by its ribose phosphate backbone.[44] Apart from the left-handed form, Z-DNA differs from A- and B-DNA in several ways: it is a slimmer helix with diameter of 18 Å, with a longer distance between the base pair residues of 3.7 Å, and its major and minor grooves have little difference (Figure 2.4 right).

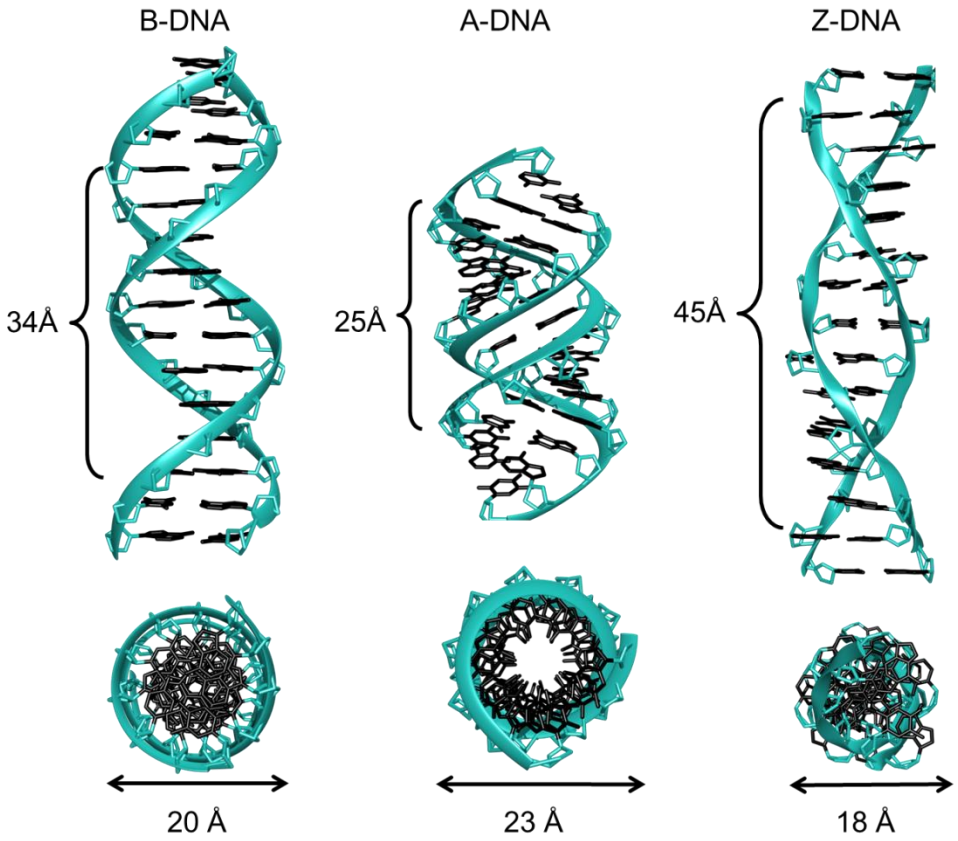

Figure 2.4 Side view, top view and dimension of double helix structure of the three forms of DNA. B-DNA (left), A-DNA (centre) and Z-DNA (right). Image was produced in HyperChem and Chimera.

2.3 DNA-Ligand Interactions

The ability of DNA to interact uniquely with many different types of molecules underpins much of the biological function and malfunction of DNA. The focus in this work is on the study of the non-covalent binding of small cationic molecules and proteins to DNA. Non-covalent interactions are fundamental to many biological structures and mechanisms. Thus, the approach of understanding molecular recognitions and the reversible interactions during the biological processes is of great importance in biophysics, physical chemistry, pharmaceutics, etc.

DNA interactions are classically based on hydrogen bonds, electrostatic interactions or van der Waal's forces. Hydrogen bonds typically form between a hydrogen donor and a hydrogen acceptor, electrostatic interactions occur between oppositely charged groups, and van der Waal's forces vary according to temporal asymmetry inherent in the electric charge distribution of atoms.

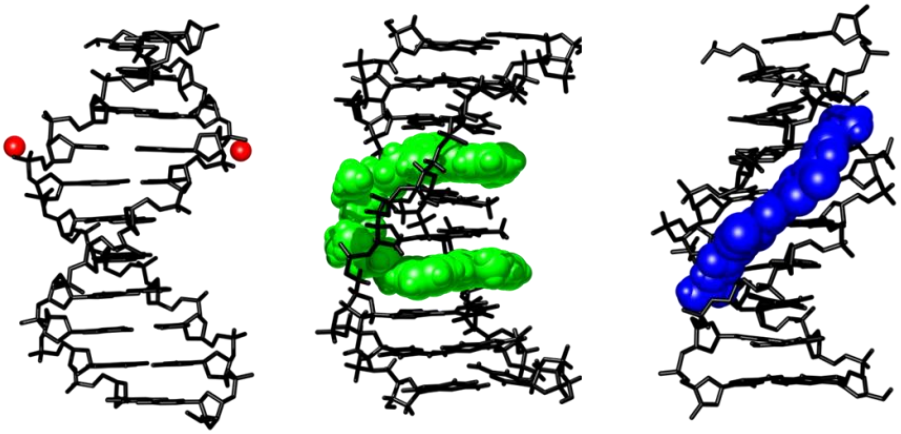

Figure 2.5 Schematic representations of the three primary binding modes for DNA-ligand binding, from left to right: electrostatic binding of counter-ions in red; intercalation of TOTO in green (PDB ID:108D);[45] and groove binding of netropsin in blue (PDB ID: 2LWH).[46]

Small molecules (ligands) primarily can bind to B-form DNA molecules in three significantly different modes. Counter-ions such as, Na^+ Mg^{2+} or polyamines bind along the exterior of the helix through non-specific and primarily electrostatic interaction with the anionic phosphate groups of the backbone (Figure 2.5 left). The bound counter-ions partially screen the charge repulsions between adjacent phosphate groups so that the duplex is stabilized. Planar or approximately planar aromatic ring systems may intercalate between two adjacent base pairs of DNA (Figure 2.5 middle). Intercalation forces the base pairs apart and causes an overall increase in the length of DNA. Intercalated ligands also induce partial untwisting of the duplex. Planar aromatic molecules with some degree of rotational freedom which are too large to intercalate may bind in the minor groove (Figure 2.5 right).[22] Large ligands such as DNA binding domains of proteins can bind to major grooves. Groove binders directly interact with edges of base pairs in grooves of nucleic acids. In real cases, certain DNA binding ligands may exhibit multiple binding modes, when the environment of interaction changes.[47]

2.3.1 Polyamines

Polyamines are a group of low molecular weight aliphatic amine organic compounds that contain two or more amino groups. Typical polyamines are putrescine, spermidine, and spermine (Figure 2.6), which are essential for cell growth from bacteria to mammalian cells.[48] Their ability for modulation of gene expression, stimulation of enzyme activity and activation of DNA synthesis prompt them to be involved in diverse and important biological processes such as regulation of cell proliferation and

differentiation have been dealt with extensively in the literature. Furthermore, polyamines have other functions that are related to DNA protection from external agents [49-51] and against radiation damage.[52-54]

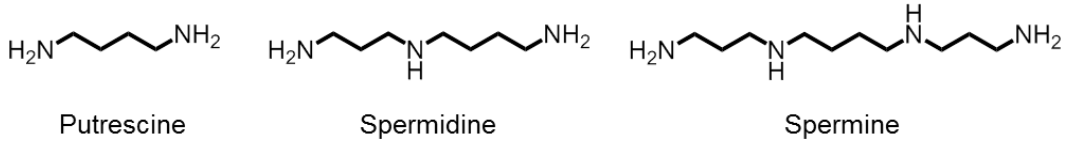

Figure 2.6 Chemical structures of putrescine, spermidine and spermine.

Since polyamines are protonated under physiological condition, they can interact with nucleic acids and specific kinds of proteins through electrostatic interactions. Interactions of polyamines and DNA have been intensively investigated.[55,56] In this thesis, spermidine and spermine were used to interact with DNA concatemers as condensation agents.

2.3.2 RAD51 Protein

The RAD51 protein is an eukaryotic protein, which assists in repairing of breaks on DNA strand. The human RAD51 (hereafter HsRad51), has 338 amino acids and a molecular weight of 37 kDa. When RAD51 assembles on single- or double-stranded DNA, each RAD51 monomer covers about three nucleotides or base pairs of DNA to produce a helical nucleoprotein filament on DNA.[57,58] Eletron microscopy and X-ray crystallography prove that the RAD51 nucleoprotein filament is right-handed helical structure, in which the DNA helix is extended by ~ 50% in length in the presence of ATP.[57,59]

2.4 Structural DNA Nanotechnology

DNA concatemers can be considered as the simplest structural DNA nanoconstructs. In many cases, when a concatemerization involves a multitude of different oligonucleotides, triplexes and quadruplexes components may also be included.[60] Sometimes their branched two-dimensional (2D) or three-dimensional DNA analogues in dendritic structure are also found for special study of interest.[61] As a matter of fact, with programmed sequences, DNA can be formed into different fancy structures. In this section, some advanced structural DNA constructs formed by artifical nucleic acids and applications are introduced.

2.4.1 Initial DNA Nanoconstructs

Nadrian Seeman, who designed and manufactured artificial nucleic acids for the nanoconstruction and used the specificity of Watson-Crick's base paring in DNA by in 1982,[62] proposed DNA with a new role in material science. The birth of DNA nanotechnology was an initial inspiration from the naturally occurring branched Holliday junction (HJ),[62] which set the foundation for structural DNA nanotechnology (Figure 2.7a left).

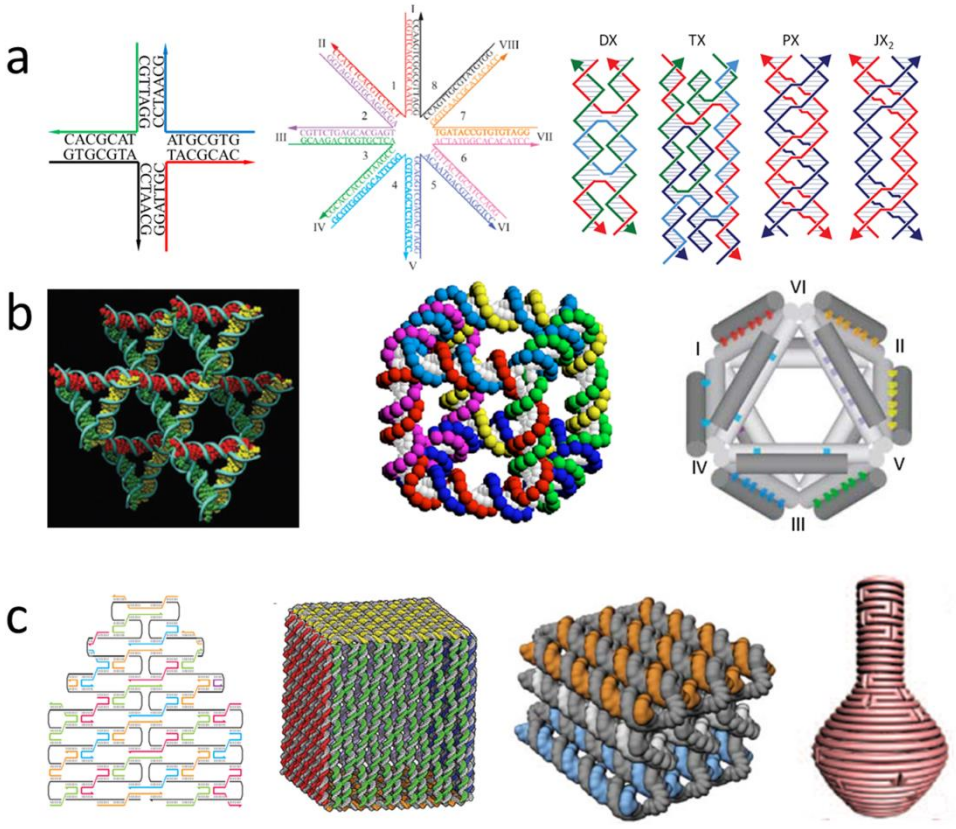

Figure 2.7 Examples of structural DNA nanotechnology. (a) 4-arm DNA junction[63] (left), 12-arm DNA junction (middle)[64], and DX, TX, PX and JX_2 motifs. (b) 3D periodic structure composed of tensegrity triangles[65](left), 3D DNA cube[66] (middle), 3D octahedron[67] (right). (c) DNA origami: 2D house-shape origami[68] (left), hollow 3D cage[69] (centre left), multi-layer square nut[70] (centre right), and nanoflask[71] (right).

Based on a similar idea, DNA junctions were developed with different numbers of arms.[64,72,73] An example of an eight-armed DNA junction is presented in Figure 2.7a middle. The development of double-cross-over[74] (DX) derived with two exchanges between double helices made the structure more rigid compared to HJ which has only one

single reciprocal exchange between double helix. The building blocks of DX tile laid the foundation for many DNA nanostructures and were further developed as TX[75], PX[76] complex and JX_2 (Figure 2.7a right).[77] The flexible branched junction structure with sticky ends makes the crossover DNA with greater rigidity and enables the assembly of even multiple lattices over the size and shape of their periodicity from DNA.[78-82] A landmark of periodic DNA structure assembly was achieved by assembly of tensegrity triangles (Figure 2.7b left)[65] to a 3D DNA crystal.[83]

At the same time, some three-dimensional individual DNA constructs were also created, for example: cube (Figure 2.7b middle)[66] and tetrahedron.[84,85] But one important development of the structural DNA nanotechnology is the use of a scaffold DNA stranded for the assembly of aperiodic structure. The first example of a scaffolding strand in structural DNA nanotechnology was a scaffolding strand made barcode lattice,[86] then DNA chain was reported as a scaffold for the assembly of a 3D wireframe octahedron (Figure 2.7b right).[67]

2.4.2 DNA Origami

In 2009, a breakthrough of structural DNA technology was demonstrated by Rothemund with the concept of "DNA origami", where a long scaffold single-stranded M13 phage genome (7.3 kilo bases) was folded with the help of 200 staple strands into defined two-dimensional shapes (Figure 2.7c left).[68] DNA origami has also been explored to extend in three-dimensiond following several strategies. One method is based on folding flat DNA origami sheets against one another into a hollow 3D cage (Figure 2.7c middle left).[69,87-89] An alternative strategy is to make a solid 3D shapes by stacking multiple layers of DNA double helices to a hexagon or square lattice (Figure 2.7c middle right).[70,90] Such a strategy was expanded to construct a rich diversity of DNA nanostructures with designed twist and curvature.[91] In 2011, a novel strategy was introduced by Han, who designed concentric rings of DNA containing different numbers of turns to generate curvature to match the rounded contours of a target container shape (Figure 2.7c right).[71] This new strategy allows researchers to construct arbitrary 3D shapes with control over the degree of surface curvature.

2.4.3 Application of DNA Nanotechnology

Three decades after Seeman's original proposal, substantial designs of DNA constructs were created for novel applications. One of the earliest applications is for structure determination, where membrane proteins were analysed by nuclear magnetic resonance (NMR) via aligning of the proteins in DNA origami nanotubes serving as detergent-resistant liquid crystals.[92] This method was then used to determine a mitochondrial membrane protein.[93] Apart from the application in determination of protein

structure, DNA constructs also have the function of organizing heteroelements, such as proteins,[82,94] peptides,[95] virus capsids,[96] and nanoparticles[97] in desired pattern or orientation. One of the remarkable applications is converting DNA from static structures into nanomachines. The active DNA started from a B-Z transition of the conformation of DNA via changing in environment.[98] Then DNA machines were driven beyond one conformational transition to perform more sophisticated tasks, for example, clocked walkers.[99] Another scenario is to apply DNA nanostructures as energy transfer devices. The ability of DNA to transport charge over a considerable distance along its bases makes DNA nanoconstructs very promising nanowires.[100-102] Two of the most feasible applications of DNA nanoconstructs are diagnostics and therapeutics. A recent study reported that a constructed DNA robot could recognize diseased cells and transport molecular payloads to them.[103] Others have used DNA origami structures as carriers for the anti-cancer drug.[104,105] With the rapid development of DNA structural nanotechnology, it is believed that a plenty of more interesting and beautiful DNA constructs will be created and DNA nanotechnology will emerge in more research fields.

CHAPTER 3

SURFACE AND DNA MODIFICATION

3.1 Self-Assembled Monolayers (SAM)

Self-assembled monolayers are formed by spontaneous adsorption of molecules on a solid surface. Figure 3.1 schematically illustrates an example of an ordered SAM assembled from long-chain alkane thiols on a gold substrate. The adsorbed molecules in SAMs usually contain three components: a head group, a spacer, and a terminal group (Figure 3.1). The head group has a special affinity to the substrate; the spacer utilizes the van der Waal's interaction to stabilize the monolayer structure; and the terminal group contributes desired functions to the modified surface.

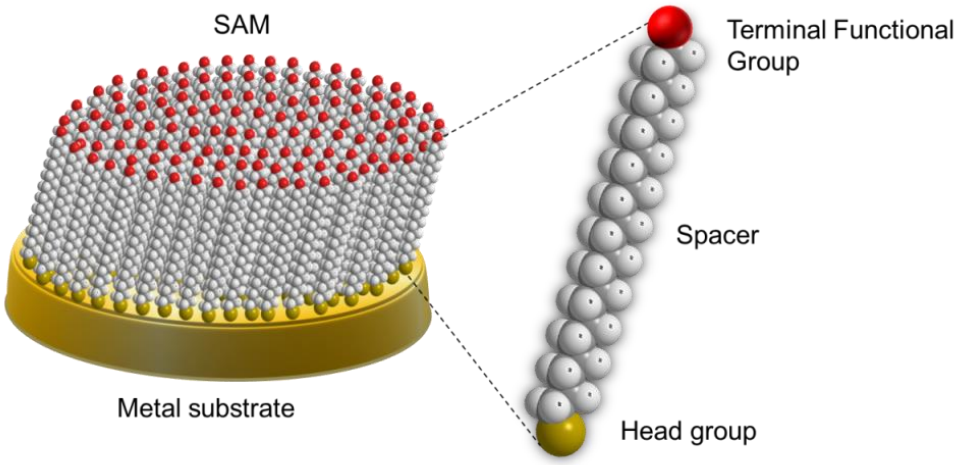

Figure 3.1 Schematic diagram of a SAM supported on a metal surface. The functional parts of an assembled molecule are highlighted in red.

The pioneer of innovation of SAM is Zisman, who first prepared a monomolecular layer by self-assembly on a clean metal surface in 1946.[106] However, the potential of SAMs was not paid much attention until Nuzzo and Allara revealed the SAMs of alkanethiolates on gold in 1983.[107] Since then SAM has been extensively studied.[108]

Based on head group-substrate affinity, different SAM molecules are prepared on varieties of surfaces. Three of the most widely studied systems of SAM are thiols on gold, silane-based systems on SiO_2 and alkanoic acids on metal oxides.

SAM offers a unique combination of physical properties that allows fundamental studies of interfacial chemistry, solvent-molecule interactions and self-organization. The well-ordered arrays, ease of functionalization, and thermodynamic stability make SAM ideal systems in many fields, where the application of the SAMs depends on different terminal groups, for example, quinone can be used for sensing pH.[109] In this thesis, biotin modified SAM provides surface binding sites for immobilizing streptavidin molecules.[110]

3.2 Biotin-Streptavidin Interactions

The streptavidin-biotin interaction is one of the strongest non-covalent bonds known until now. Due to the high binding affinity (K_a = 2.5 × 10^{13} M^{-1})[111] and specificity between biotin and streptavidin, the strong interaction has been applied in many fields.[112]

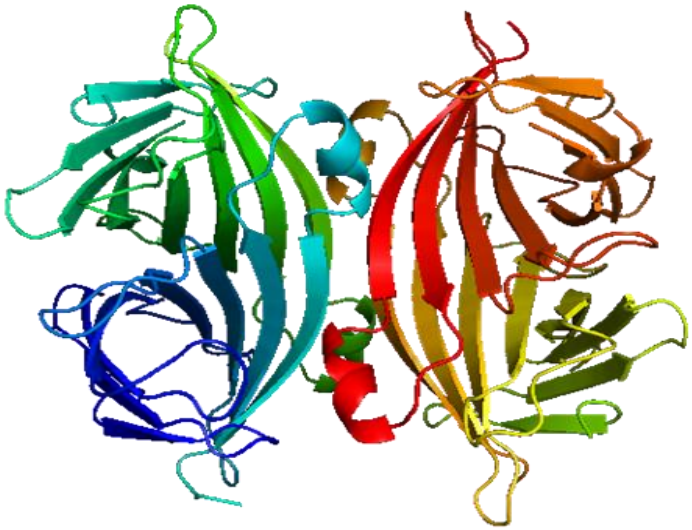

Figure 3.2 Crystal structure of tetramer structure of streptavidin. (PDB ID:1SWB).[113]

Streptavidin is a tetrameric protein with a molecular weight of approximately 60 kDa, with a mildly acidic isoelectric point (pI) of 5-6, which is purified from the bacterium *Streptomyces avidinii* (Figure 3.2). Each streptavidin molecule contains four identical subunits, which can bind strongly to one biotin.[114] The X-ray crystal structure suggests that the geometry of streptavidin is approximated by a cube with the side length of 5.4×5.8×4.8 nm.[115]

Biotin, otherwise known as vitamin H, is a small molecule (244 Da) that carries carboxyl groups and functions as a co-factor for catalyzed carboxylation or antibody binding. The carboxyl group of biotin is the site attached to ε-amino groups of lysine residues through an amide bond. When biotin is introduced to biological macromolecules such as proteins, polysaccharides or nucleic acids, the biological activities of these molecules are generally not affected because biotin is very small.

3.3 Chemically Modified Oligonucleotides

Chemically synthesized oligonucleotides usually carry a series of nucleotides, as well as free hydroxyl groups at the 3'-end and/or 5'-ends. Oligonucleotides that contain extra chemical group other than the normal bases are called modified oligonucleotides. These modifications can be positioned at the 3'- or 5'- end of the oligonucleotide, or internally within the backbone or at the nucleobases.

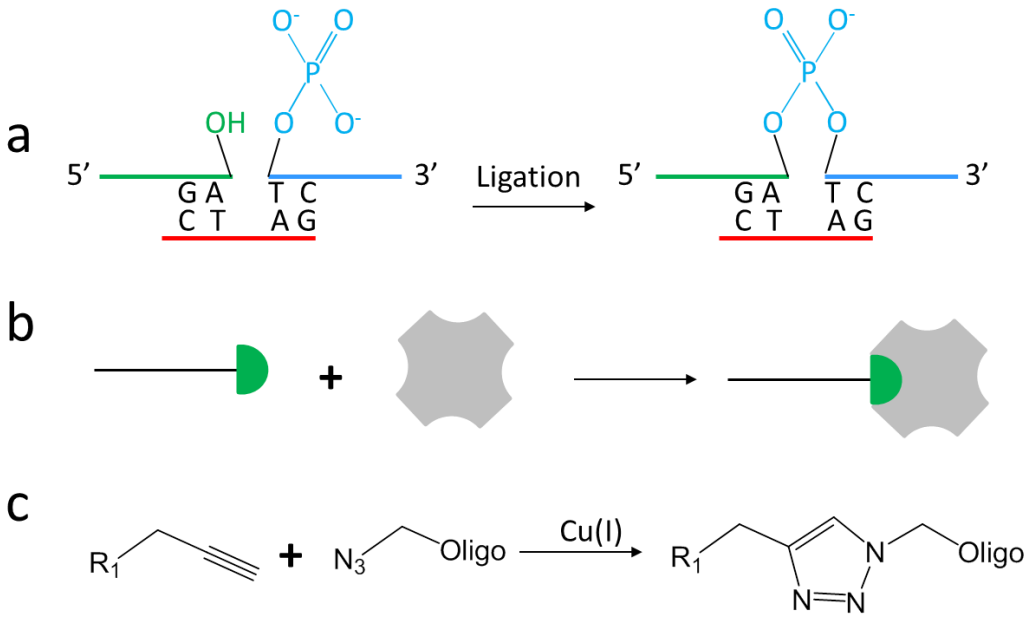

Figure 3.3 Schematic representation of chemically modified oligonucleotides and their applications. (a) 5'-phosphorylated oligonucleotide in a ligation reaction; (b) a biotinylated oligonucleotide binds to a streptavidin; (c) a click chemistry modified oligonucleotide in a cycloaddition reaction.

Modified oligonucleotides are used in various applications due to the properties of modified moieties. In this thesis, three types of chemically modified oligonucleotides are used to form concatemers, including phosphorylated, biotinylated, and click chemistry labelled oligonucleotides. Figure 3.3 exhibits the modified oligonuleotides and their uses. Oligonucleotides with 5'-phosphate group are utilized in ligation reaction to join two strands of oligonucleotides together to form a longer DNA strand (Figure 3.3a).

Biotinylated oligonucleotides can be attached to streptavidin-enzyme-conjugates, to streptavidin-protein-conjugates, to strepavidin-coated surfaces or to streptavidin-dye-conjugates, since biotin has highly specific affinity towards streptavidin (Figure 3.3b). Click chemistry reaction is an organic method to join small units together. An important example is azide-alkyne cycloaddition via using Cu^{I} as catalyst to seal DNA (Figure 3.3c).[116]

CHAPTER 4

THEORY AND METHODOLOGY

4.1 Absorption Spectroscopy

Absorption spectroscopy is a fundamental optical technique that measures the absorption of radiation when the energy of light is absorbed by matter. Figure 4.1 schematically displays a setup of spectrophotometer for measuring absorption spectra.

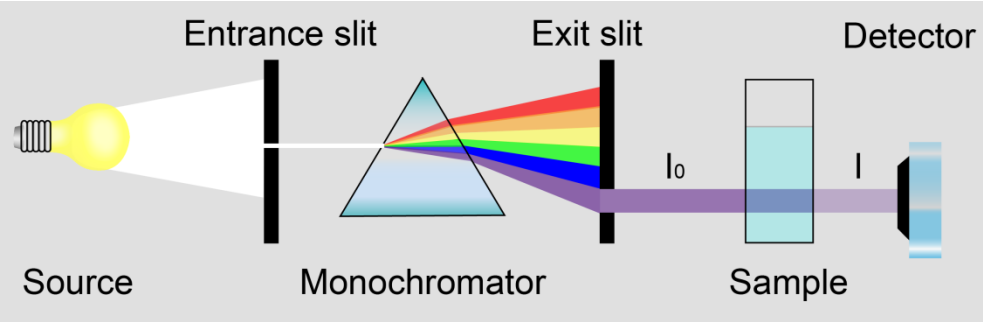

Figure 4.1 Schematic drawing of a spectrophotometer and its major components.

When light is shining through a sample, the intensity of light decreases after passing through sample solution ($I_0 \geq I$) because of the interaction between light and the sample molecules. Light is commonly described either as an electromagnetic wave or as discrete photons with energy, $h\nu$, where h is Planck's constant, and ν is the frequency of the light. When a molecule in an initial ground electronic state (S_0) is exposed to light, it may absorb a photon and make a transition to a higher energy state (S_1) if the frequency of the light satisfies the gap between the two energy states of the molecule according to

$$\Delta E = h\nu \tag{1}$$

where ΔE represents the energy difference between the two states. In general, transitions between electronic states correspond to absorption of light in the ultraviolet and visible range, while transitions between vibrational or rotational states correspond to absorption of light at longer wavelengths (infrared or microwaves).

Practically, absorption is used to measure the concentration of molecules using the Beer-Lambert law

$$A = \log \frac{I_0}{I} = \varepsilon \cdot c \cdot l \tag{2}$$

where A is the absorbance, I_0 and I are the intensities of the incident and transmitted light, respectively, ε is the extinction coefficient of a molecule at certain wavelength, c is the concentration of measured solution, and l is the optical path length of sample cell. For DNA molecules, a distinct absorption peak typically occurrs around 260 nm.

4.2 Gel Electrophoresis

Gel electrophoresis is an expeimental method for detecting, separating, and purifying a mixture of particles or macromolecules. When an electric field is applied to a gel matrix containing charged molecules, the charged molecules will move towards one of the electrodes (i.e. a net positively charged molecule moves towards the cathode, conversely a net negatively charged molecule moves towards the anode) through the gel, and be separated depending on the rate of movement of each component. The motion of charged particles or molecules relative to a solution under the influence of an applied electric field is defined as electrophoresis.

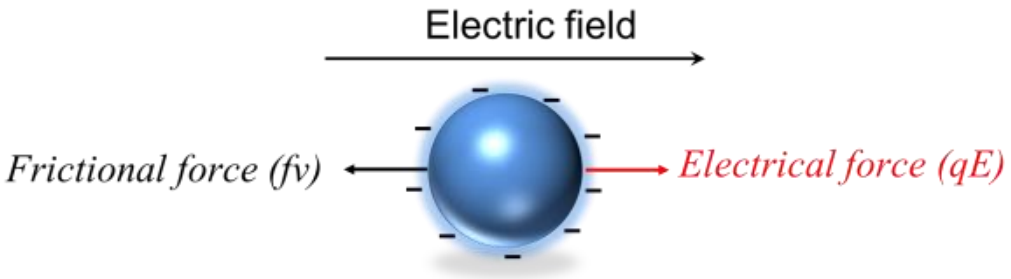

Figure 4.2 Illustration of electrophoresis: a negatively charged particle experiences an electrical force and frictional force.

Figure 4.2 depicts the force diagram of a net negatively charged particle in electrophoresis. The charged particle is exposed to an electric force as an acceleration force, which depends on the charge of the particle (q), and the strength of the electric field (E). At the same time, the particle also experiences a frictional force in the opposite direction to the electrical force. The frictional force is related to the velocity of the particle (v) and the frictional coefficient (f), which depends on the size and shape of the particle. When the velocity accelerates to a certain value, the accelerating and the retarding force

are equal. In this circumstance, the rate of the motion per unit of field strength is called the electrophoretic mobility (μ):

$$\mu = \frac{v}{E} = \frac{q}{f} \tag{3}$$

where q is the net charge of the particle, E is the electric field, f is the frictional coefficient, v is the velocity of the particle, and the electrophoretic mobility μ is velocity per unit electric field. The difference in electrophoretic mobility among macromolecules is used for seperation.

In principle, electrophoresis can be executed in free solution; however, to get an efficient separation, gel matrix with pores are nearly always used to in all cases of electrophoresis experiments to analyse macromolecules in order to reduce mixing of the molecules by convection and diffusion. A gel is a three-dimensional polymer network dispersed in a solvent. Two common types of gels for electrophoresis are agarose and polyacrylamide. The former contains polysaccharide obtained from agar which is suitable for separating large molecules; whereas the latter is made by copolymerization of acrylamide and bisacrylamide which is often used for separating smaller molecules. In addition, it is found that circular DNA molecules can be trapped in polyacrylamide gel.[117] gel. The pore size of the gel can be adjusted by increasing or decreasing the percentage of gel content.

Many biological macromolecules are charged; therefore they could migrate in the presence of an electric field. For example, nucleic acids are polyelectrolytes that carry multiples of individual negative charge (from the phosphate group) at physiological pH. The charges of nucleic acids are linear proportional to their molecular length. Thus, a sample of mixed sizes of DNA can be separated by their lengths in gel electrophoresis. Proteins, on the other hand, are amphoteric molecules that can carry positive, negative or zero net charge depending on each amino acid residue at varied pH. Each protein has its own isoelectric point which is a specific pH at which the net charge is zero. Therefore, using isoelectric focusing, proteins can be separated in gels with pH gradient. Alternatively, making proteins denatured in sodium dodecyl sulfate (SDS) polyacrylamide gel can separate proteins by their molecular weights.

4.3 Atomic Force Microscopy (AFM)

Scanning Probe Microscopy (SPM) is a new family of microscopy techniques that obtains images by scanning a sharp probe across a surface and measuring the probe-surface interaction. The two primary forms of SPM are Scanning Tunnelling

Microscopy[118] (STM) and Atomic Force Microscopy[119] (AFM), both invented by Binning and co-workers. The STM measures the tunneling current (using a conducting surface), and the AFM measures the forces acting between a fine tip and a sample. Thus, AFM is a development of STM that can image the shape of an insulating sample surface with very high resolution in three dimensions with details down to the nanometer scale.

Figure 4.3 displays the basic concept of an AFM setup, with the three main components labeled as a piezoelectric tube (PZT) scanner, a sharp tip (probe) attached to the free end of a pliable cantilever, and a photodiode detector. The probe is positioned above the surface of a sample. When the probe raster scans across the sample surface, the attractive or repulsive force resulting from interactions between the probe and the surface will cause a positive or negative bending of the cantilever. The bending is then detected by a laser beam, which is reflected on the back side of the cantilever into the photodiode detector. Simultaneously, the PZT scanner records the precise position movement of the probe in the x, y, and z dirctions with nm resolution. A 3D topography of the sample surface is subsequently obtained.

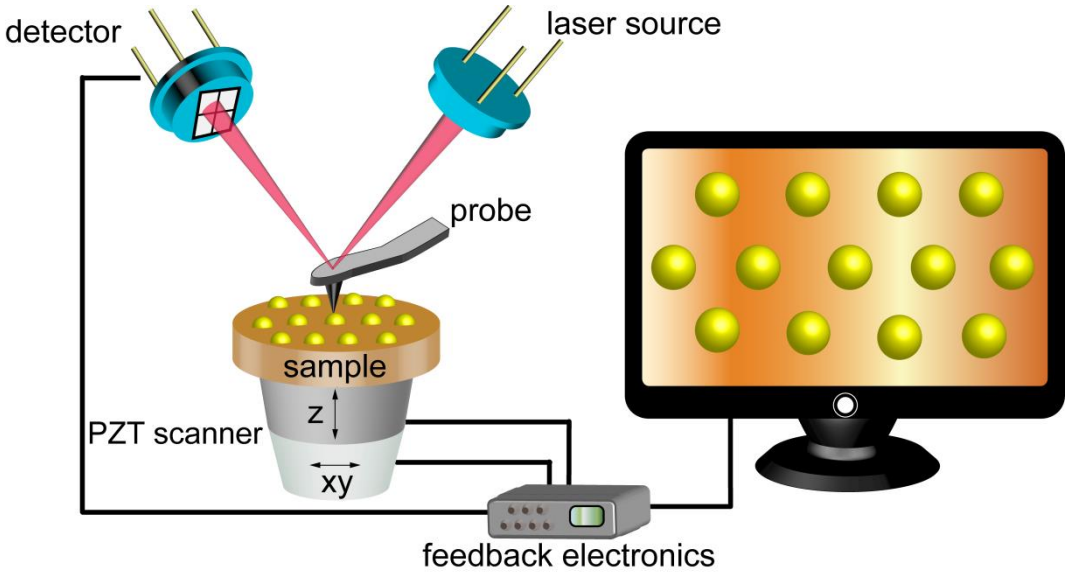

Figure 4.3 Schematic illustration of the basic components in an AFM setup.

To obtain a surface image the AFM tip is approaching down to the surface. As mentioned, AFM senses the interactions between the tip and the sample surface. The interactions depend on the van der Waals' force upon probe-sample distances (Figure 4.4). There are three major regions of interaction between the probe and the surface: when the probe is far from the surface, there is no interaction between the tip and the surface (Figure 4.4 in green); and this region is called free space; as the probe is approaching the surface, it enters the attractive region and is pulled downwards (Figure 4.4 in blue); and

when the probe is “touching” the surface, it experiences in the repulsive region and is deflected upwards Figure 4.4 in red).

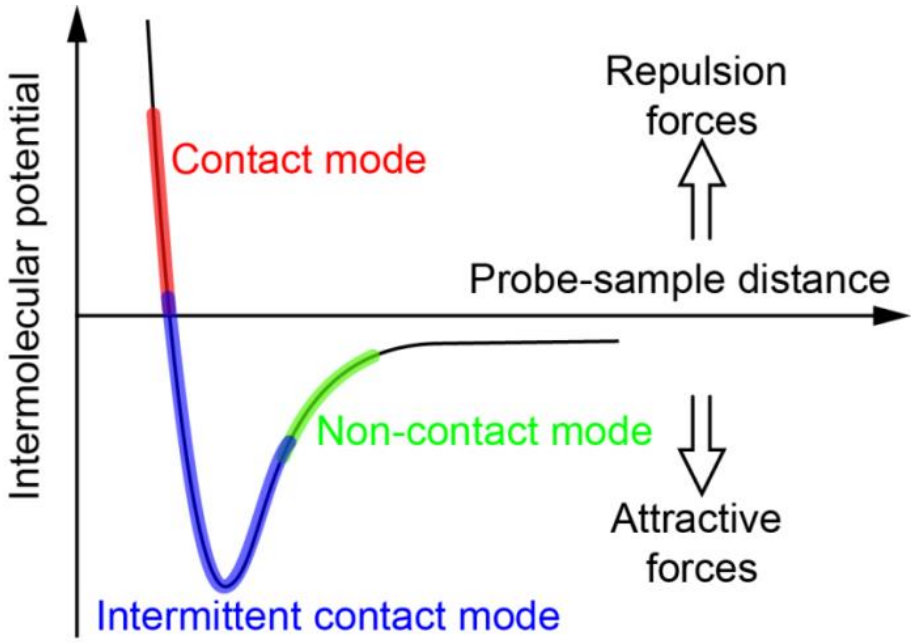

Figure 4.4 Lennard-Jones potential diagram of the attractions and repulsions between a probe atom and a sample atom.

There are three imaging operations of AFM: contact mode, intermittent contact mode (tapping mode), and non-contact mode (Figure 4.5). In contact mode, the probe scans either at a small constant height above the surface or under the condition of a constant force. In the former situation, there would be a risk that the probe would collide with the surface and cause damage of probe or sample. Hence, the most commonly used mode is constant-force mode. In this case, a feedback is involved from the PZT, when the probe scans across the sample surface the resulting deflection due to the z position is measured (Figure 4.5 left). In tapping mode, the cantilever is externally oscillated at its resonance frequency above the sample surface. By maintaining a constant oscillation amplitude, the resonance frequency will shift due to the attractive force between the probe and sample (Figure 4.5 middle). Changes in the frequency provide information of the surface characteristics. Tapping mode is used for biological samples in most cases because of less damage of surface. In non-contact mode, the probe oscillates above the surface the same way as in tapping mode, but not touching the sample surface at all (Figure 4.5 right). Since the probe-sample distance is further than 10 nm, the interaction force is quite low. The detection is also based on the measuring of changes to the resonant frequency or amplitude of the cantilever.

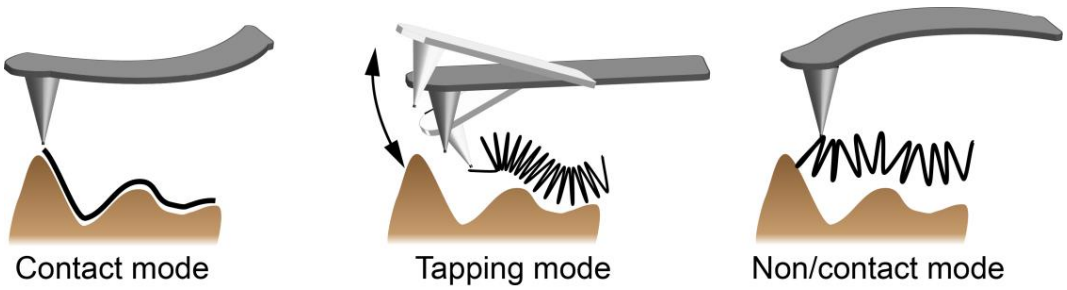

Figure 4.5 Scheme of imaging modes: contact mode (left), tapping mode (middle), and non-contact mode (right).

AFM has several advantages over electron microscopy. Insulating samples do not require to be pretreated with metal or carbon coating. It can operate in a vacuum, air or even liquid environment. In addition, it provides a three-dimensional image of a sample. The main disadvantage of AFM is the single scan image size; however the AFM can only show an image with a maximum height by micrometres and with a maximum area by 100×100 micrometres.

4.4 Quartz Crystal Microbalance with Dissipation Monitoring (QCM-D)

Quartz crystal microbalance (QCM) is an acoustic surface sensing method used to measure mass per surface area by detecting the change in resonance frequency of a quartz crystal resonator. A QCM sensor consists of a thin quartz crystal disc with a metal electrode deposited on each side (Figure 4.6). Relying on an inverse piezoelectric effect, an AT cut crystal shear oscillates when an alternating current is applied to the electrodes. Upon addition of a small mass on a QCM sensor surface, a decrease in the resonance frequency is induced. In 1959, the German scientist, Günter Sauerbrey first demonstrated that the adsorbed mass (Δm) on the quartz surface is linearly proportional to the change in resonance frequency (Δf).[120] This linear relation between Δm and Δf is therefore often referred to as the Sauerbrey equation:

$$\Delta m = \frac{-C \cdot \Delta f_n}{n} \tag{4}$$

where C is the mass sensitivity constant (17.7 ng·Hz^{-1}·cm^{-2} for a 5 MHz crystal), Δf_n is the frequency shift for a given harmonics (overtone) number n (n=1, 3, 5, 7, 9, 11, 13…)

Figure 4.6 Illustration of a common gold covered QCM sensor, i.e. an AT-cut quartz crystal disc with a gold electrode deposited on each side: top view (left), bottom view (right) of the sesnor and the electrode deposited on top of the quartz disc. Left one is the surface which is used for sensing. Right one shows the electrode on the opposite side of the sensor. The present configuration of the electrodes allows contacting of the sensor form this side.

This linear relation typically holds for thin, rigid films in vacuum and air when the the following assumptions are fulfilled: the adsorbed mass is small compared to the mass of the crystal and the adsorbed layer is evenly distributed on the crystal surface as a rigid film. Since 1980, QCM has also been utilized in the liquid phase.[121] In liquid, the mass detected by QCM also includes any liquid trapped in or associated with the adsorbed film. Moreover, non-rigid films in which the adsorbed viscoelastic molecules do not fully couple to the oscillating surface caused more rapid damping of the oscillation and the Sauerbrey equation could not be applied. These problems motivated new developments of the technique as a tool to characterize such films.

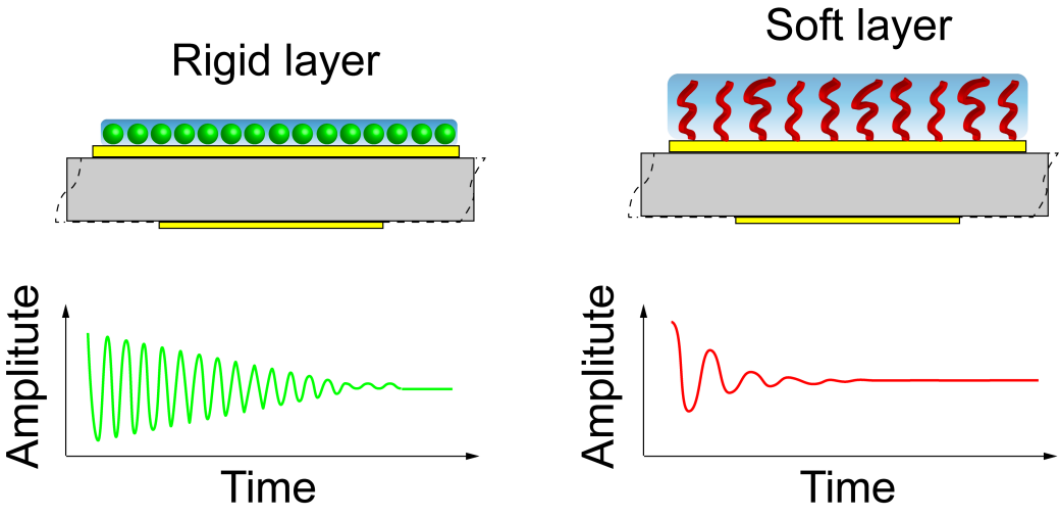

Figure 4.7 Schematic illustration showing how the oscillation of a QCM-D crystal depenss on the properties of an adsorbed film. The resonance frequency decreases as more mass is coupled to the sensor, and the disspation is lower for a rigid (left) compared to a soft (right) film. Figure inspired from technology note QS 407-01-2, Biolin Scientific.

The quartz crystal microbalance with dissipation monitoring (QCM-D) technique is a variant of QCM where simultaenously to the measurement of the resonance frequency of the sensor, the dampening of the oscillatory motion (referred to as dissipation) is also

quantified. The dissipation is measured by periodically switching on and off the driving voltage and observing the decay time (τ) of the oscillation amplitude. The energy dissipation is a dimensionless quantity defined as the ratio of energy loss (E_{lost}) during one oscillation cycle to the total energy stored in the oscillating system (E_{stored}).

$$D = \frac{1}{\pi f \tau} = \frac{E_{lost}}{2\pi E_{stored}} \tag{5}$$

By measuring dissipation, the softness of an adsorbed film can be estimated, or from the acoustic ratio ($\Delta D/\Delta f$).[122,123] A rigid film is characterized by a low, relative ΔD value, whereas a soft film has a higher relative ΔD value (Figure 4.7). Spreading of the recorded frequency and dissipation data when measured at different overtones is an alternative method to distinguish a soft layer from a rigid layer for which the response is insensitive to overtone number. To quantitatively analyse the viscoelastic properties of the adsorbed films that is beyond Sauerbrey regime, a Voigt-based viscoelastic model[124] can be used to derive the effective thickness (δ_F), shear elastic modulus (μ_F), and shear viscsity (η_F) of the viscoelastic films from frequency and dissipation measurement at multiple overtones (Figure 4.8).

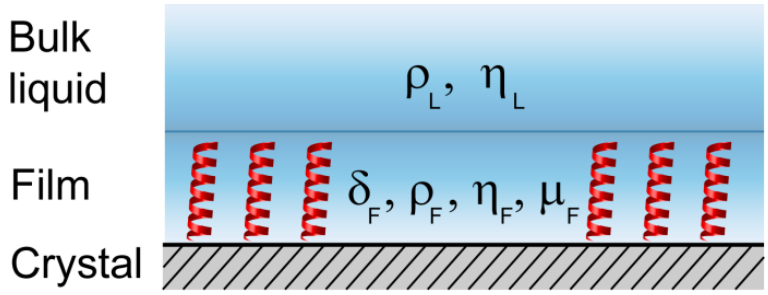

Figure 4.8 Schematic of a QCM-D crystal covered with a single uniform viscoelastic adsorbed film in a bulk liquid. The bulk liquid is a viscous material with density ρ_L and shear viscosity η_L, and the layer is a viscoelastic material with density ρ_F, shear elastic modulus μ_F and shear viscosity η_F.

4.5 Surface Plasmon Resonance (SPR)

Surface plasmon resonance (SPR)-based sensing techniques rely on changes in optical properties, i.e. changes in the refractive index (RI), near a sensor surface. A surface plasmon (SP) is a charge-density wave (a collective oscillation of electrons) that propagates along the interface between a metal surface and the ambient medium. Since

the wave appears on the boundary of the metal and the ambient, the oscillation is very sensitive to any change of this boundary, for example, by adsorption of biomolecules.

The discovery of the SPR phenomenon dates back to 1902 by Wood,[125] who first observed anomalous reflective patterns by shining polarized light on a mirror with diffraction grating on its surface. Physical interpretation of this phenomenon was initiated by Lord Rayleigh,[126] but a complete explanation was not demonstrated until 1968 by Otto,[127] and in the same year Kretschmann and Raether[128] reported the excitation of surface plasmon by attenuated total reflection (ATR) using an optical setup. In 1982, Nylander and Liedberg utilized SPR for gas detection and biosensing.[129,130] Since then, SPR has emerged and established as a highly powerful label-free analytical technique for monitoring biomolecular interactions.[131]

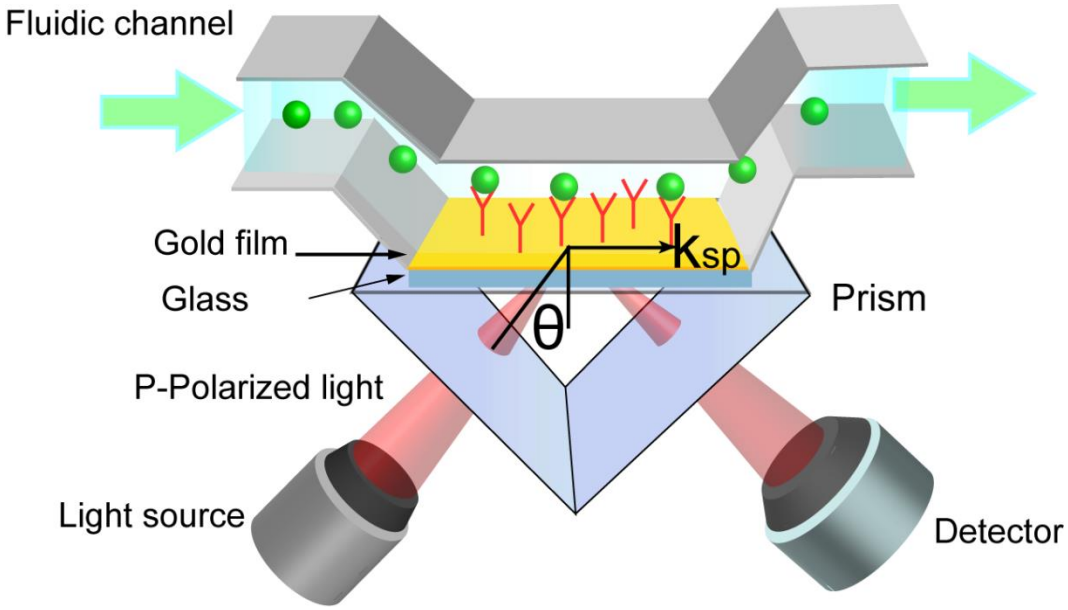

Figure 4.9 Schematic illustration of the Kretschmann configuration for optical excitation of SPR. A sensor chip with a gold coating is placed on a prism. Polarized light shines from the light source on the sensor chip. Reflected light intensity is measured in the detector. When the angle θ is larger than a certain critical value, energy is transferred from the light into the surface plasmon and SPR occurs. Figure inspired from Roh.[132]

The most commonly used set-up for SPR-based sensing is the so-called Kretschmann configuration (Figure 4.9). The Kretschmann geometry is based on total internal reflection. When polarized light is applied through a prism from the backside of a sensor chip with a thin, semitransparent noble metal film, the light will be reflected by the metal film performing as a mirror. Total internal reflection occurs when the incident angle increases to a critical angle (θ_c). The SP is excited at an angle θ_{sp}, when a small part of the light may

penetrate across the interface as an evanescent field and excite a surface plasmon wave. At resonance, the surface plasmon wave vector k_{sp} equals the component of the incident light wave vector parallel to the prism interface k_x ($k_{sp}=k_x$) leading to

$$k_{sp} = \frac{2\pi}{\lambda}\sqrt{\frac{\varepsilon_m \varepsilon_s}{\varepsilon_m + \varepsilon_s}} \tag{6}$$

$$k_x = \frac{2\pi}{\lambda} \tag{7}$$

where k_{sp} is the surface plasmon wave vector, λ is the wavelength of light, ε_m is the dielectric constant of the metal film, ε_s is the dielectric constant of the surrounding media, and k_x is the component of the incident light wave vector parallel to the prism interface.

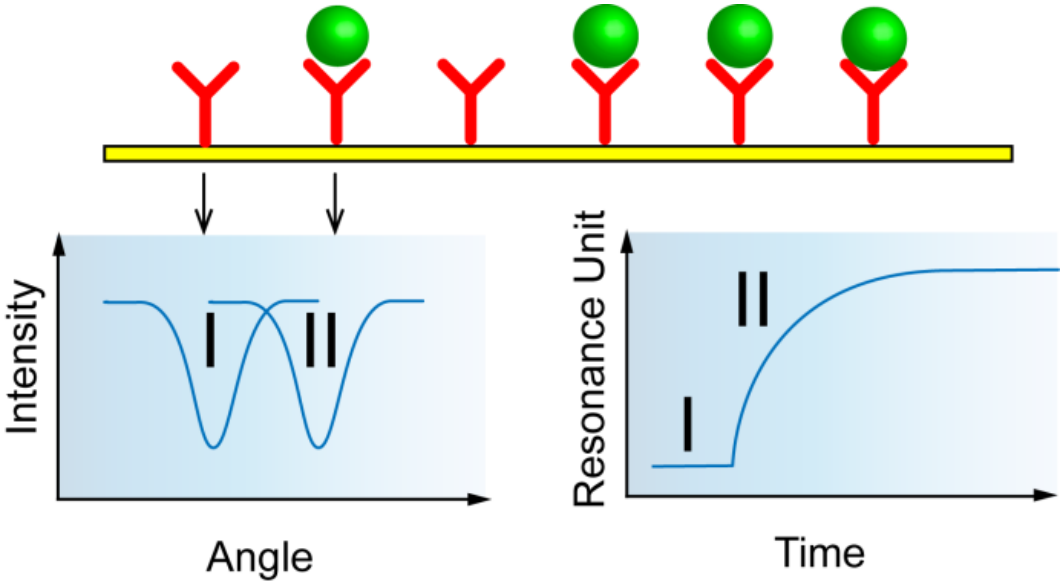

Figure 4.10 In SPR-based sensing, binding of biomolecules results in a shift of the angle at which the "SPR-dip" in the intensity of the reflected light occurs (left). This change in resonant angle is monitored in real time versus time (right).

The intensity of the reflected light will decrease when the condition for surface plasmon resonance is fulfilled, thereby, SPR is observed as a characteristic dip in the intensity of the reflected light. The refractive index at the prism side is constant, but the refractive index in the immediate vicinity of the metal surface will be changed due to association or dissociation of biomolecules. At the same time, the surface plasmon wave vector, k_{sp}, which is dependent on the refractive index of the sample medium close to the

metal surface, is altered; and consequently, the shift of the SPR angle (θ) is measured (Figure 4.10 left).

The monitoring of the resonance angle, θ, as a function of time allows for detailed analysis of, e.g., binding events at the surface. In the instrument used in this thesis, the recorded signal is quantified in resonance units (RU) (Figure 4.10 right).

CHAPTER 5

RESULTS AND DISCUSSION

The main goal of this thesis is to form linear DNA constructs in terms of concatemers for studying DNA-ligand interaction at single DNA level. To enhance the ligand binding possibilities, long strands of dsDNA with repetitive sequences series are preferred. Although extracting long linear DNA molecules from nature is not difficult, chromosomal DNAs with particularly desired and repetitive sequences cannot be easily found in nature. In this chapter, the formation and characterization of assembled DNA concatemers achieved in *Paper I-IV*, as well as some preliminary unpublished results of relevance, are summarized and discussed.

5.1 Assembly of DNA Concatemers

5.1.1 Assembly of DNA Concatemers in Bulk Solution

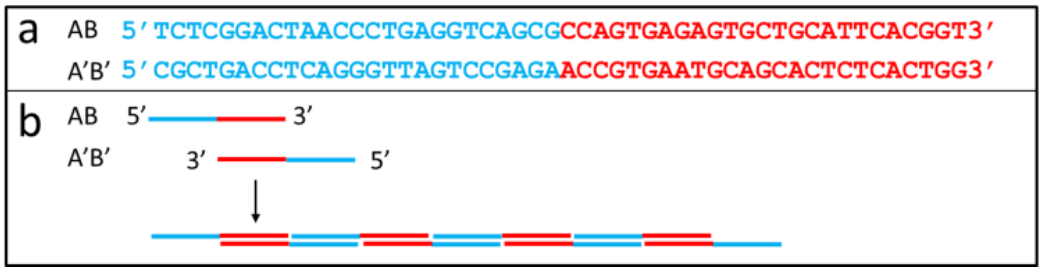

Figure 5.1 (a) Sequences of the semi-complementary 50 base pair oligonucleotides AB and A'B'. (b) Formation of concatemeric DNA duplexes by hybridization of AB and A'B'. The sequence of the 3'-half of the AB-strand (in red) is complementary to the sequence of the 3'-half of the A'B'-strand (also in red). These halves of AB and A'B' can thus form a 25 base pair duplex (red in the bottom part in Figure. 5.1b).

According to Seeman's proposal for DNA nanoconstructs fabrication,[62] it is not a difficult project to form linear structual DNA constructs via DNA self-assembly, if the sequence of oligomers are properly designed. Following this strategy, we designed two strands of oligonucleotides with 50 bases each, mutually semi-complementary to each

other, for forming DNA concatemers (Figure 5.1). In particular, their sequences were designed for studying the binding of actinomycin D to DNA.

The strands are named AB and A'B', where the part A, B, A', and B' each contains 25 bases, whereby A is complementary to A', and B is complementary to B'. It is important to point out that oligonucleotides AB and A'B' are not completely complementary, but semi-complementary to each other during the hybridization due to the antiparallel characteristic of two DNA strands. Therefore, the free end of single strands make the concatemer extendable when hybridizing to a new strand (Figure 5.1).

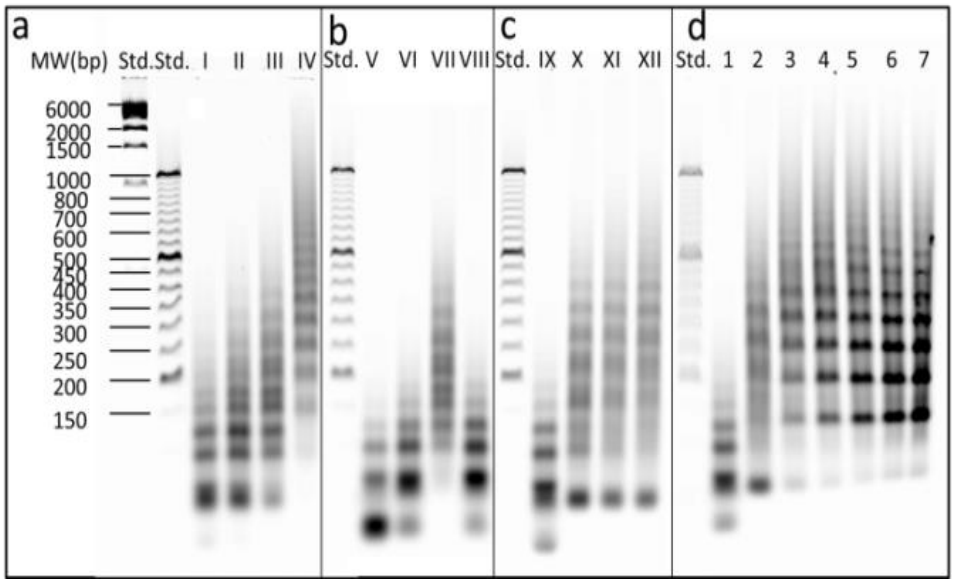

Figure 5.2 Electrophoretic gel analysis of the DNA concatemers assembled under various conditions. (a) Oligo concentrations: 2.5, 5, 10 and 20 µM strands (lanes I-IV), with all samples incubated at 20°C for 2h before the electrophoresis. (b) Incubation temperature: 4, 20, 37 and 60°C (lanes V-VIII), at 2.5 µM oligo for 2h. (c) Incubation times: 2, 24, 48 and 72 hours (lanes IX-XII), at 2.5 µM oligo at 20°C. (d) Added salt: 0, 25, 50, 100, 200, 300 and 400 mM NaCl (lanes 1-7), at 2.5 µM oligo, at 20°C for 2h. During concatemer formation all samples contained a background phosphate buffer (5 mM, pH 7.6); only in panel (d) was the ionic strength higher. Electrophoresis in 2.5% non-denaturing agarose gels at 4V/cm. In panel (a) two overlapping size standards (Std) are indicated by the size of the fragments in base pairs. The gels in panels (b)-(d) only contained the shorter size standard.

To obtain long concatemers, oligonucleotides were hybridized in bulk solution under several conditions via varying oligomer concentrations, temperatures, duration of incubation, and ionic strengths (Figure 5.2a-d). The gel electrophoresis images in Figure 5.2 suggest that concatemers are always formed with a certain size distributions in length. In addition, long concatemers (> 300 bp) are found to form preferably in conditions of

prolonging incubation time or increasing reaction rate in different ways, such as increasing the concentration of oligonucleotides. Increasing incubating temperature could also assist to form long concatemers; however, it is important to keep the incubation temperature below the melting temperature of DNA. Most of all, adding salt to around 200 mM NaCl was found to be the most efficient way of forming concatemers (Figure 5.2d).

The concatemers are designed to increase their lengths by adding 25 base pairs content in each step. It is seen that DNA concatemers in a native gel migrate with different speeds, compared to the standard ladders with known lengths, because the extendable end of the concatemers together with the nicks on the backbones might influence the mobilities of concatemers in a non-denaturing gel. In order to compare the size of concatemers with standard ladders without tail effect, the best correction is to ligate the concatemers and run them in a denaturing gel (Figure 5.3a). In this way, the effect of nicks can also be ignored. Results reveal that after ligation, the mobilities of concatemers in gels are in good agreement of with standard ladders. Surprisingly, the lengths of the concatemers in the denaturing gel are much shorter than they are in native agarose gels, suggesting that the ligation was not efficient. To confirm that this result is caused by a non-efficiency of the ligation, a series of heating-cooling-ligation (HCL) cycles were used to ligate concatemers to a better extent (Figure 5.3c).

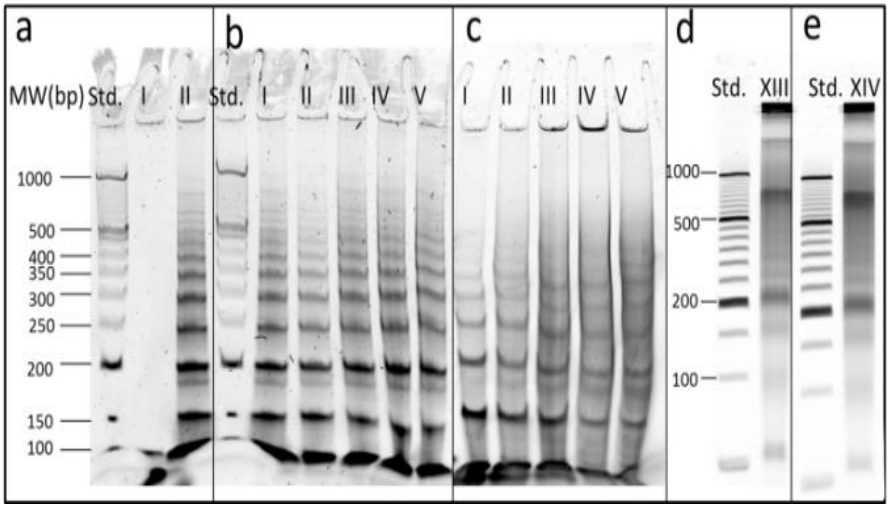

Figure 5.3 Polyacrylamide gel electrophoresis (PAGE) of the concatemers. Gels in panels (a) - (c) are denaturating PAGE (7M urea; 50°C), gels in panels (d) and (e) are native PAGE. (a) Non-ligated (I) and ligated (II) concatemers. (b) and (c): Oligonucleotides underwent one to five heating, cooling and ligation cycles (denoted I-V), either with excess of ligase and kinase (b) or with a stoichiometric amount of enzymes (c). (d) and (e): native 5% PAGE at 22.5V/cm either in constant field (d) or in pulsed inversion field electrophoresis (e). Sample in (d) and (e) are the same sample as used in (a).

In a native polyacrylamide gel, a large portion of the formed DNA concatemers is stuck in the well (Figure 5.3d). To our understanding, the DNA molecules migrated in the gels are in linear shape, whereas molecules stuck in the gel wells are non-linear or too large to enter into the gel. A non-linear structured concatemer could be formed during ring formation by intramolecularly hybridizing of two ends within one molecule when the backbone of the concatemers become very flexible. Results suggest that the non-linear products are not simply circles (Figure 5.3e), because circular DNA should migrate in the gel when running in field-inversion gel electrophoresis.[117] Thus, those stuck molecules might be in complex structures.

AFM images provide more direct evidences that the assembled DNA molecules are in a large size range. Figure 5.4a displays spread objects which are most likely DNA molecules because the height of DNA detected in experiment (Figure 5.4d) is consistent with previous AFM measurment of DNA in air.[133] Large, single and entangled molecules are also observed using AFM (Figure 5.4b and c), which reveals why some molecules are stilll trapped in a pulsed field electrophoresis (Figure 5.3e).

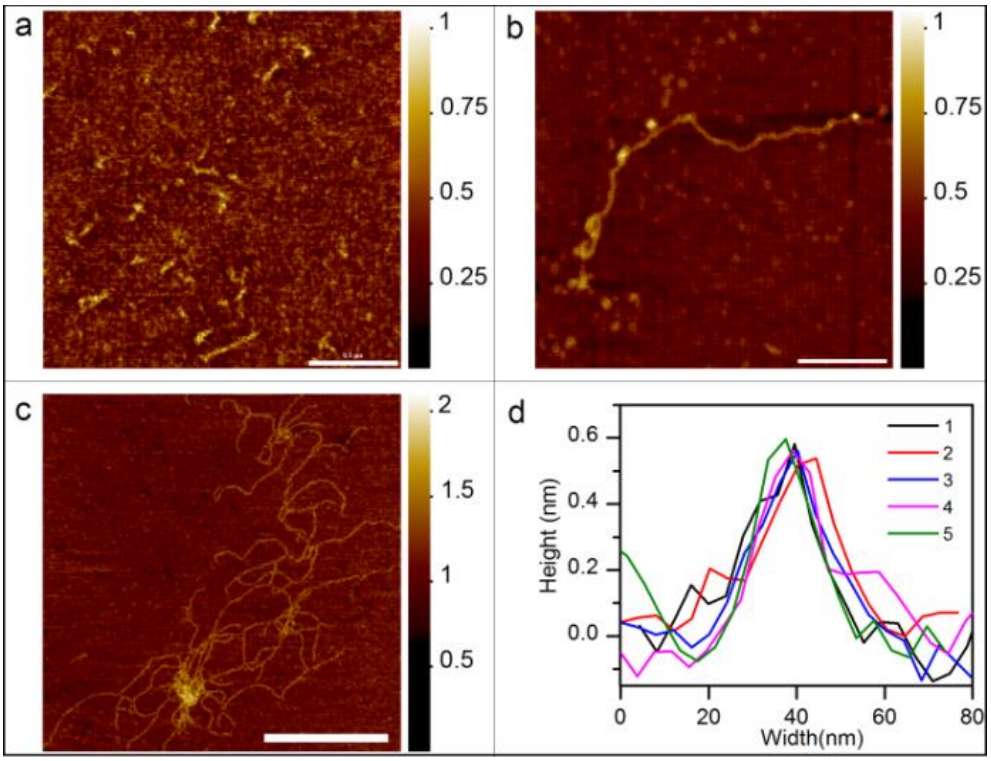

Figure 5.4 AFM images of the hybridization products. Panels (a), (b) and (c) images in air showing the variation in the tertiary structure of the hybridization products. a) short constructs; b) longer and slightly entangled products; c) large and highly entangled products. d) typical height profiles of 5 individual constructs. The location of the profiles in panel a) can be found in supporting information. The scale bar is 0.5 µm in (a), 0.25µM in (b) and 1µm in (c).

For future studies of DNA-ligand interactions at the single-molecule level, linear concatemers could be separated from the mixture of various shaped products using native polyacrylamide gel electrophoresis, thereafter the linear concatemers could be purified by cutting and eluting from the gel.

5.1.2 Assembly and Release of DNA Concatemers on a Planar Surface

Although the concatemers formed by self-assembly in bulk solution manner (*Paper I*) are long enough for single-molecule experiments, a serious drawback of this method is the difficulty of controlling the size and the shape distributions of the concatemers for future studies on single-molecular manipulation. One solution is to avoid the formation of non-uniform and non-linear concatemers via inactivating the circular formation by attaching one end of the concatemers on a planar surface and hybridizing oligonucleotides stepwisely, to form the concatemers until reaching an expected length.

The platform was designed to immobilize the first single-stranded DNA to a streptavidin monolayer, and then to construct concatemers stepwisely by hybridization. The first experiment of alternatingly hybridizing A'B' and AB to a biotinylated AB monolayer showed that hybridizing with AB led to nearly no response in QCM-D. A complete hybridization probably occurred between one A'B' and two neighbouring biotinylated AB, which failed the establishment of a platform. To develop a platform for constructing concatemers in a continuous fashion, a short oligonucleotide A' is introduced to make DNA layers extendable.

Table 1. Oligonucleotides for assembly of concatemers.

Name	No. of bases	Oligonucleotide sequence from 5′ to 3′
b-AB_{59}	59	biotin-TTTTTGATCTCTCGGACTAACCCTGAGGTCAGCGCCAGTGAGAGTGCTGCATTCACGGT
A'_{34}	34	CGCTGACCTCAGGGTTAGTCCGAGAGATCAAAAA
A'B'	50	CGCTGACCTCAGGGTTAGTCCGAGAACCGTGAATGCAGCACTCTCACTGG
AB	50	TCTCGGACTAACCCTGAGGTCAGCGCCAGTGAGAGTGCTGCATTCACGGT
A	25	TCTCGGACTAACCCTGAGGTCAGCG

To release the concatemers from the surface, the oligonucleotides were designed to have additional cleavage site. A 59-mer oligonucleotide (b-AB_{59}) and a 34-mer oligonucleotide (A'_{34}), instead of b-AB and A', respectively, were introduced for the subsequent cleavage experiment, which contains a 5-mer (A/T) spacer and a 4-mer (GATC) sequences for restriction enzyme to recognize. All oligonucleotide sequences used in this study are listed in Table 1, in which b-AB_{59} is designed to immobilize on a streptavidin-modified surface, the same building blocks as the bulk assembly method, oligonucleotides AB and A'B' are used in the sequential method for assembly of the

concatemers, and a 25-mer oligonucleotide (A) is used to complete the whole concatemer double stranded, till the top.

The process of sequential hybridization was monitored using QCM-D. Figure 5.5 displays the measurement of the first five steps of sequential hybridization of DNA concatemers on a QCM-D sensor. The result reveals a step-by-step hybridization of oligonucleotides, indicating that a surface-based platform for assembly of DNA concatemers is established.

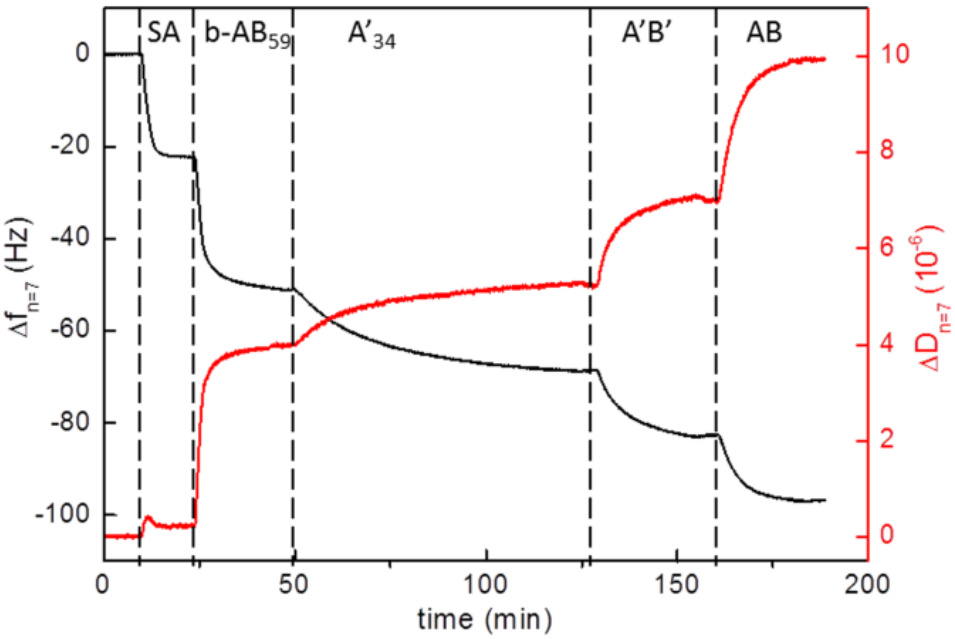

Figure 5.5 A real time QCM-D measurement showing changes in the resonance frequency Δf (black, left axis) and dissipation ΔD (red; right axis) during the first five assembly steps, using the 7th overtone. Measurements at other overtones, 3rd, 5th, 9th and 11th, exhibited similar trends. The zero level for Δf and ΔD corresponds to the biotinylated gold surface before binding of streptavidin (SA).

Following the establishment of the sequential hybridization platform, DNA concatemers of different lengths were constructed in separate experiments, each monitored using QCM-D. The concatemers were then trimmed off the surfaces and run in gel electrophoresis to investigate their size distributions. Clear bands at expected position in comparison with standard ladders can be found in the electrophoresis image, which strongly indicates that the concatemers were successfully constructed by this method (Figure 5.6A). However, some by-products consisting of concatemers longer than the expected lengths can also be found in the gel. After running temperature ramp experiments on QCM-D, it is believed that those by-products were probably formed during the cleavage process, where concatemers could partly melt and rehybridize to different lengths at 37°C due to the non-ligated nicks.

Table 2. Oligonucleotides with click chemistry moieties for assembly of concatemers.[a]

Name	No. of bases	Oligonucleotide sequence from 5′ to 3′
b-A'$_{34}$-c	34	X-CGCTGACCTCAGGGTTAGTCCGAGAGATCAAAAA-biotin
c-AB$_{59}$	59	TTTTTGATCTCTCGGACTAACCCTGAGGTCAGCGCCAGTGAGAGTGCTGCATTCACGGT-X
c-A'B'	50	X-CGCTGACCTCAGGGTTAGTCCGAGAACCGTGAATGCAGCACTCTCACTGG-Y
c-AB	50	Y-TCTCGGACTAACCCTGAGGTCAGCGCCAGTGAGAGTGCTGCATTCACGGT-X
c-A	25	Y-TCTCGGACTAACCCTGAGGTCAGCG-X
c-B'	25	X-ACCGTGAATGCAGCACTCTCACTGG-Y

[a.] *b is short for biotin, c is short for clickable, X is alkyne and Y is azide.*

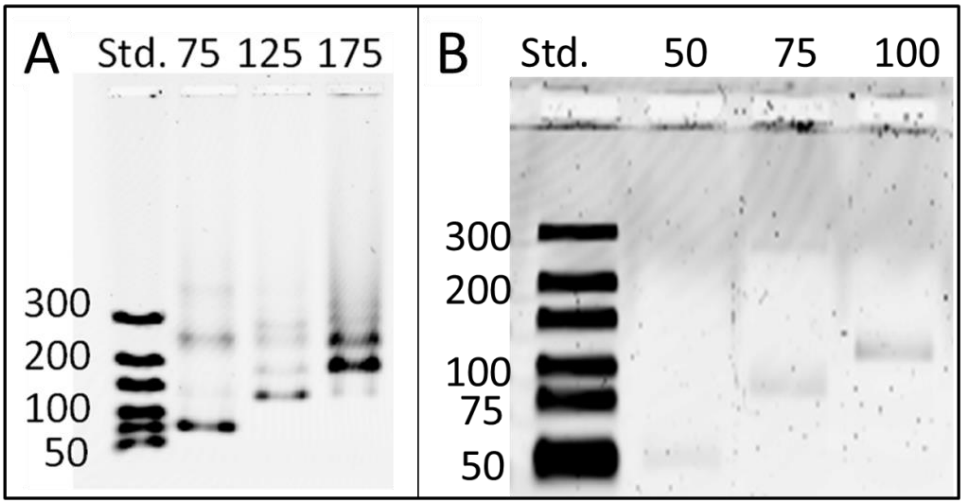

Figure 5.6 Gel electrophoresis images of trimmed-off concatemers and standard ladders. (A) Non-ligated concatemers in 4% agarose gel. (B) Clicked concatemers in 10% native polyacrylamide gel. Numbers at top indicate the expected DNA length. Std is size standards with indicated number of base pairs.

To avoid redistribution of the concatemers during the cleavage process, click chemistry reaction is introduced to seal the nicks on the backbone of concatemers at room temperature instead of using ligation at 37°C. Oligonucleotides with the same sequences as used in previous studies were modified with click chemistry moieties at the backbone ends for new experiment (Table 2). Click reactions were performed after each hybridization step, whenever a nick is needed to be sealed. Clicked concatemers were trimmed off surface and run gel electrophoresis to characterize the length (Figure 5.6B). The results confirm that each sample corresponds to a single band at its own expected length, which strongly indicates that the concatemers retain the same length as when assembled on the surface. It is also observed that the shortest concatemer is at the expected position compared to the 50 bp band in the standard ladder, while concatemers with 75 bp and 100 bp migrate slightly slower than corresponding size standard. The

slower migration of clicked concatemers might be because of the non-charged triazole-linker which replaces the phosphate charge from the phosphodiester bond in the native DNA ladder.

5.1.3 Modelling of Concatemer Multilayer

QCM-D has the advantage of providing the viscoelastic properties of a soft layer on the sensor surface. An optical method such as SPR, on the other hand, gives an estimate of the biomolecular mass of the layer. In *Paper III*, sequential hybridization experiments were also studied on SPR to obtain the DNA mass. Using the sequential hybridization platform, a 534 bp DNA concatemer layer was constructed, monitored, and characterized using QCM-D and SPR (Figure 5.7).

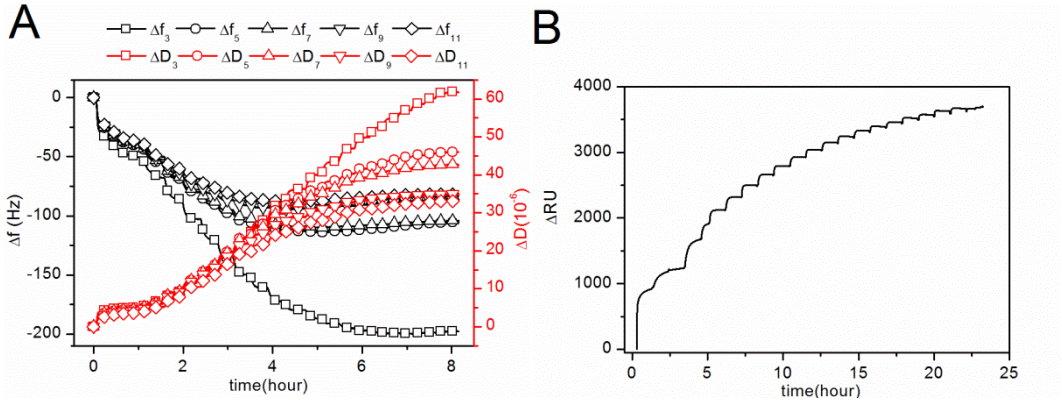

Figure 5.7 (A) QCM-D measurements and (B) SPR sensorgram of the stepwise assembly of a 534 bp synthetic double-stranded DNA multilayer. Changes in frequency (Δf) and dissipation (ΔD) versus time are shown at indicated overtones n. The first step in the QCM-D as well as in the SPR result corresponds to the biotin-DNA being immobilized to the streptavidin surface.

In the QCM-D measurement, changes in frequency (Δf) show a pattern of negative-zero-positive changes as the number of steps increases, while dissipation increases monotonously (Figure 5.7A). This result confirms the theoretical prediction that frequency and dissipation changes will not always follow a linear trend during a multilayer adsorption experiment in QCM-D.[124] Using the Voigt-based modelling, the viscoelastic properties of the concatemer layer were characterized together with SPR. Results suggest that the DNA layers are highly viscous and that the water content of the DNA layer is about 90%. Figure 5.8 displays the modelled data for the DNA layer, where the thickness increases in a monotonous fashion at each hybridization step, whereas the effective shear viscosity exhibits a marked maximum at the third step.

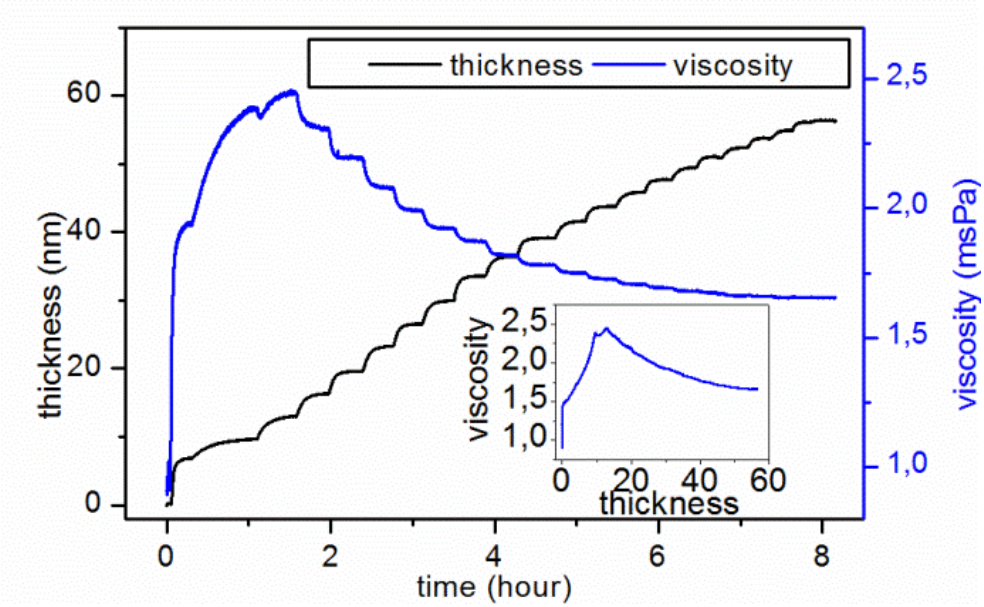

Figure 5.8. Changes in effective thickness (black; left axis) and effective shear viscosity (blue; right axis) versus time during the step-wise DNA-assembly as obtained from the Voigt-based modelling shown in Figure 5.7A. Insert graph shows the plot of effective viscosity versus effective thickness.

The negative-zero-positive changes in Δf were previously observed in multilayers of 100 nm liposomes.[134] To better understand the non-linear viscoelastic behaviour of a polymer film, a 3084bp concatemeric DNA layer was assembled and its QCM-D response was compared to the calculated data by Voigt model of a 1µm-think polymer film (Figure 5.9). The calculated results suggest that changes in Δf and ΔD at different overtones have strongly non-monotonous dependences on the DNA length, with a linear pattern only occurring when the layer is thin (Figure 5.9A below 200 nm). Experimental data (Figure 5.9B) indicate an initial decrease in Δf following by upward turning during the construction of longer concatemers. After about 850bp (Figure 5.9B at 15 hour), an essentially constant response is observed despite of continued sequential hybridization. Furthermore, a predicted turning point of ΔD (Figure 5.9) is not seen in the experiments, either. A comparison between calculated data and experimental data in terms of a plot of ΔD versus Δf (see *Paper III*) suggests that the modelling is in relatively good agreement with the expected results for thin DNA layers. For thick DNA layers, formation of DNA coils due to the flexibility might prevent the layer from linearly increase in thickness with the DNA contour length, or the coils could result in a decrease in hybridization efficiency. Therefore, predictions for polymer films containing DNA duplexes up to several hundred base pairs became less consistent with experimental data.

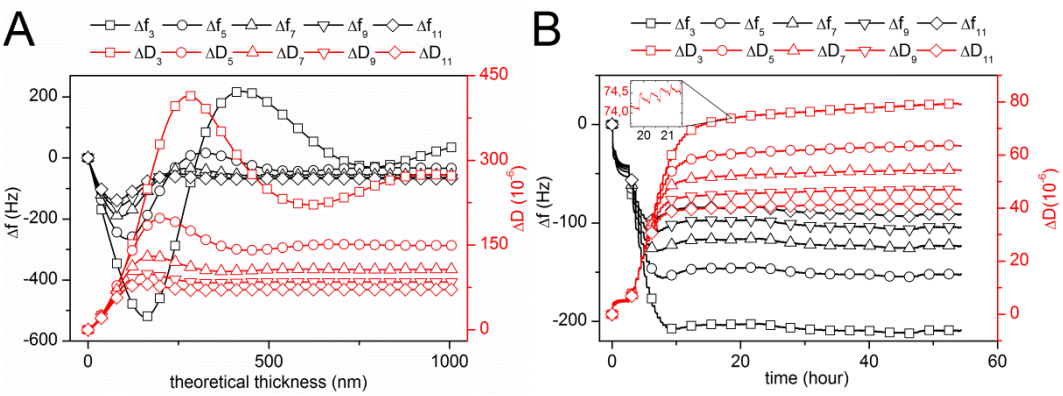

Figure 5.9 (A) Calculated changes in Δf and ΔD versus layer theoretical thickness for a DNA layer up to 1μm in thickness, using the Voigt-based model. (B) QCM-D measurements during the stepwise assembly of a 3084bp DNA layer.

5.2 DNA Concatemers-Ligand Interaction

The capability of monitoring and estimating the viscoelastic properties of a DNA film assembled onto surfaces via QCM-D measurements and the Voigt-based modelling provide potential in DNA biosensor design and development. As is well known (see section 2.3), DNA conformation may change when interacting with ligands or proteins. In *Paper IV*, QCM-D and modelling of the recorded data were utilized to detect conformational change during DNA-ligand binding. Two types of molecules were selected in this study: cationic polyamines (spermidine and spermine) and the RAD51 protein, which are known to condense and extend DNA, respectively. Both types of molecules were also studied with SPR to measure the bound biomolecular mass. Interactions between DNA concatemers longer than 200 bp and polyamines were not used in this study since the results in *Paper III* showed that non-linear responses in QCM-D for thick layer could lead to complicated interpretation.[124]

In addition, the assembly of concatemeric DNA layers in this study was improved with better duplex formation than in the previous study (*Paper III*) by reducing the surface coverage of immobilized DNA. Characterization of hybridization efficiency in *Paper III* suggested that when A'_{34} hybridizes to b-AB_{59}, the efficiency is only about 57%. Similarly, low hybridization efficiency was also found in a previous study of immobilizing DNA on a streptavidin layer and subsequent hybridization with the complementary strand.[26] The hybridization efficiency is enhanced via reducing the surface coverage of biotin-DNA in this study. In *Paper IV*, the probe density was reduced by prehybridized b-AB_{59} and A'_{34} in solution to streptavidin layer, and by manually interrupting the immobilization when the desired surface coverage was reached.

5.2.1 Polyamine Induced DNA Condensation

For studying DNA-polyamine interactions, concatemeric DNA layers containing 59 bp, 84 bp, 159 bp, and 184 bp were individually formed on separate sensors via sequential assembly on sensor surfaces as mentioned in the previous sections. An example of the overall signal upon an 84 bp layer formation followed by polyamine interaction with this layer recorded by QCM-D is displayed in Figure 5.10 at overtone n=5.

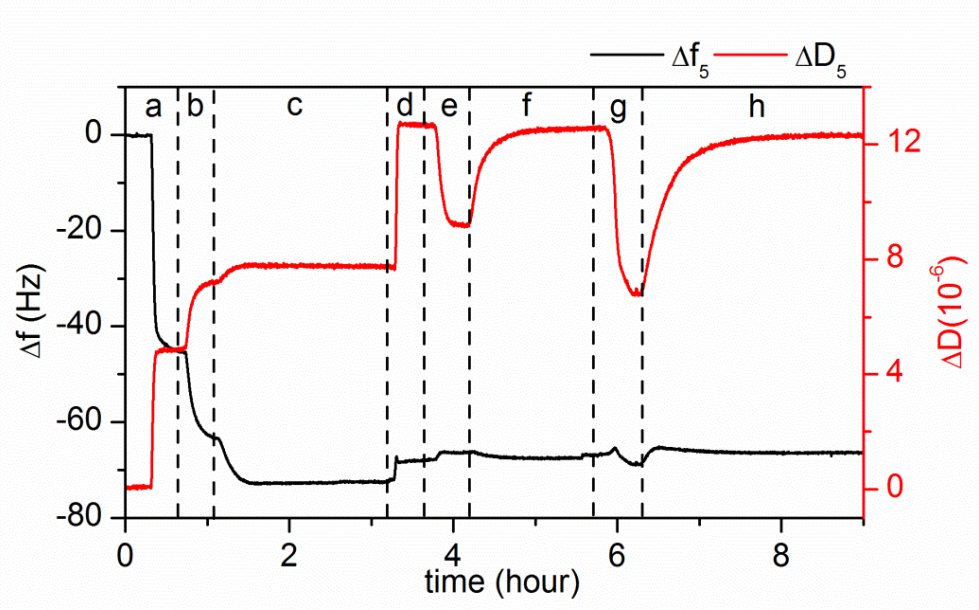

Figure 5.10 Shifts in frequency Δf (black) and dissipation ΔD (red) (at overtone n=5) versus time measured by QCM-D during the formation of an 84bp DNA layer on a preformed streptavidin-modified surface, and the subsequent interaction with the polyamines. DNA assembly by subsequent additions of (a) prehybridized b-BA_{59} and A'_{34}, (b) A'B' and (c) A in 1xPBS, followed (d) by a change to 0.07xPBS buffer, (e) addition of spermidine, (f) rinsing with ligand-free 0.07xPBS, (g) addition of spermine and (h) buffer rinsing.

The layers with different DNA lengths had similar responses upon polyamine association, but with some differences due to effects of the penetration depth. Formation of DNA layers was performed in 1xPBS buffer (Figure 5.10a-c), while interactions with polyamines were performed in diluted 0.07xPBS buffer (Figure 5.10e-f). As seen in Figure 5.10, changes in frequency (Δf) and dissipation (ΔD) show similar responses upon formation of DNA layers compared to the previous study (*Paper III*).

During the spermidine interaction, a slight positive increase in Δf upon spermidine binding to the DNA layers suggests that some mass was released from the layer. Simultaneously a clear decrease in ΔD indicates that the layer became thinner and stiffer (Figure 5.10e). Increased Δf points out that some of the water contained within the DNA layer has been removed, while decreased ΔD implies that the layer has become rigid. This

result is consistent with the knowledge from bulk experiments that spermidine condenses DNA[55,56] so that the spermidine bound DNA layer is expected to become thinner and closer to the surface. Upon rinsing with buffer (Figure 5.10f) the frequency and dissipation values return to the same level as measured for the native DNA layers, which demonstrates that the binding of spermidine to DNA is reversible. The recovered DNA films were used to study the binding of spermine. A stronger decrease in ΔD is seen when spermine bind to DNA layer (Figure 5.10g), which indicates that an even thinner DNA layer is formed by the condensation with spermine compared to that of spermidine, and in addition, dissociation of spermine is slower than with spermidine (Figure 5.10f and h).

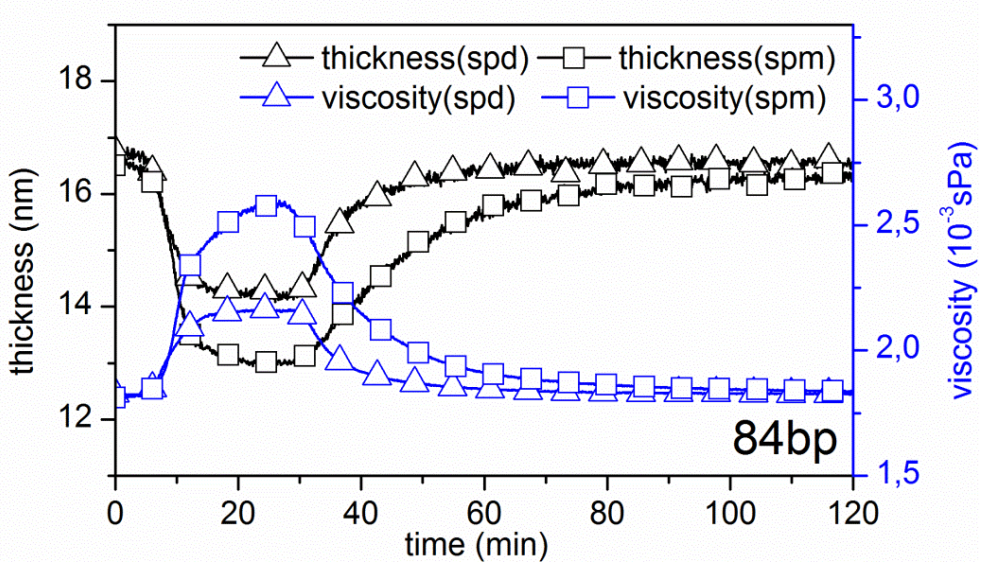

Figure 5.11 The effect of spermidine (triangles) and spermine (squares) on the effective thickness (black) and shear viscosity (blue) of DNA films with lengths of 84 bp. The polyamines were added at t = 10 min, polyamine-free 0.07xPBS buffer at t = 30min

Effective viscoelastic properties evaluated by the Voigt-based model clearly state that the layer thicknesses decrease, while the layer viscosities increase upon individual binding of spermidine and spermine to the DNA films (Figure 5.11). For example, for the 84bp DNA layer, the thickness reduced from ~16.6 nm to 14.2 nm and 13.0 nm when binding to spermidine and spermine, respectively (Figure 5.11). These results imply that both polyamines condense DNA strands so that the DNA layer decrease in thickness and become more rigid. The stronger effect of spermine on both parameters confirms that it condenses the DNA films to a larger extent than spermidine, which is most probably due to the higher positive charge of spermine (4+) compared to spermidine (3+) leading to a stronger binding to DNA by electrostatic interactions.

5.2.2 RAD51 Induced DNA Extension

To investigate if QCM-D could also be used to detect DNA film expansion, the interaction between DNA and a protein called RAD51 was investigated. The protein RAD51 is known to form a right-handed helical filament around DNA and thereby extending the helix by approximately 50%.[57,59] A DNA layer containing 59 bp in length was used for this study with an even lower surface coverage to reduce the crowding-effect[135] so that the proteins have enough space to bind to the DNA layer.

The QCM-D results show that the binding of RAD51 is a very slow process in spite of the reduced DNA coverage. Viscoelastic modelling demonstrates that the thickness of DNA layer increases from 7.6 nm to 22 nm when bound to the RAD51 protein, which is more than the expected extension of 50% in bulk experiments.[57] It could be a result of the DNA strands not only being extended along the backbones but also reoriented by rising up from the surface. Moreover, the modelled viscosity suggests that the interaction of RAD51 with DNA layer is a two-phase binding, where the first step could be related to reorientation of the tilted DNA duplexes upon binding to the RAD51, while the second phase is perhaps a slower rearrangement of the RAD51 molecules among the DNA molecules.

CHAPTER 6

CONCLUDING REMARKS

Single-molecule methods are rapidly developing for studying the mechanics of DNA-ligand interaction. However, the nonexistence of chromosomal DNA with only desired and repetitive sequences and the difficulty to produce such long synthetic oligonucleotides have limited investigations of DNA-ligand interaction at the single-molecule level. The presented study is aimed to explore methods for assembly of linear DNA concatemers to study ligand binding to DNA using optical tweezers.

A direct way to self-assemble concatemers is studied after designing the sequences of the oligonucleotides by simply mixing the different components. Linear DNA concatemers of desired lengths formed in this way are purified using native polyacrylamide gel electrophoresis, following steps of cutting the wanted gel piece and eluting DNA from the gel. Due to the wide distribution of sizes and structures found in the assembled mixture, a large amount of molecules is lost during the purification procedure. Accordingly, although self-assembly of oligonucleotides in solution has some drawbacks such as low yield of linear concatemers, yet, it is considered as a feasible method to form DNA concatemers.

In order to investigate a better way to construct only linear structured DNA concatemers, a platform of sequential-assembly of concatemer on surface is established and studied using QCM-D and SPR. Hybridization efficiency on the platform is improved by introducing hybridization of a half complementary single strand and reducing surface density of immobilized DNA. To allow collection of formed DNA concatemers, the immobilized strand is designed with a cleavable site at the bottom of the DNA layer. Although the platform is generally thermal stable, yet rehybridization occurred during the restriction process. This difficulty is overcome by connecting backbones via click chemistry at room temperature. After all these improvements, the surface-based assembly platform becomes a practical tool to build DNA concatemers. In addition, as a concatemers assembly method, the platform is combined with monitoring using QCM-D, which, in turn, for the first time, provides a relative continuous model system to utilize QCM-D and the Voigt-based modelling to characterize detailed viscoelastic properties of a thick DNA film. Results demonstrate that the Voigt-based model provides reliable information regarding thickness, viscosity, and shear modulus for short DNA layers;

however, thicker DNA films do not behave as predicted by a simple rigid rod molecular model, which is probably a result of nonlinear growth in thickness caused by helix coiling.

This research work also brings QCM-D and also SPR to the table as methods to detect DNA conformational changes. Using the established surface-assembly platform, short DNA layers with different lengths are individually formed and interacted with multi-cationic polyamines or the RAD51 protein for ligand-induced DNA deformation studies on QCM-D. Measurement and modelling of QCM-D data suggest that the DNA layer became thinner when bound to polyamines, while the addition of the RAD51 protein resulted in a thicker layer, which are both consistent with the knowledge that polyamines and RAD51, condense and extend DNA, respectively in solution. Furthermore, the native DNA layers are regenerated by removing the bound ligands in this study, which can be useful when comparing the effects of an unknown analyte with a known substance as reference.

In summary, two powerful methods for DNA concatemers construction are described: self-assembly in free solution and sequential-assembly on planar surface. Both methods could successfully form DNA concatemers up to several hundred base pairs in length. Each method has its own merit; the former is time efficient in the presence of high salt concentration, while the latter is structure predictable and length controllable. Moreover, the surface-based platform combined with QCM-D (and likely also SPR) monitoring provided a biosensing method to detect conformational changes in DNA, which can be useful to study the conformational change of DNA when bound to other ligands.

CHAPTER 7

ACKNOWLEDGEMENTS

The work presented in this thesis is not a product of one person alone. It would have not been possible without the support of many caring people. I am greatly indebted to all of the individualls who have contributed directly and indirectly to this work or my graduate experience as a whole.

I would first like to thank my supervisor, Professor **Björn Åkerman** for giving me consistent encouragement, patience, guidance and support throughout my Ph.D studies. Thank you for teaching me to think and solve problems in critical and scientific way.

Also I am very grateful to Professor **Bengt Nordén** for the support to make this thesis possible. Thanks for the interesting disucssion in each Marathon meeting.

I also must extend my thanks to my co-supervisors **Sofia Svedhem** and **Fredrik Westerlund** for great discussion and technical supervision on my research work.

Karolin Frykholm and **Louise Fornander**, thank you for your invaluable contribution to the projects.

I want to thank **Nils Carlsson**, **Niklas Bosaeus** and **Pegah Nabavi** for sharing the lab and stimulating discussions.

My (ex) office-mates, **Hans-Christian**, **Lena**, **Mélina**, **Anke**, **Tamas**, **Jong-Ah**, **Jakob**, **Nesrine,** and **Masoumeh**, thanks for giving very nice office atmosphere.

I would like to thank people at physical chemistry and biological physics.

Appreciations to **Nesrine, Niklas, Nisse, Laura, Pegah, Sandra,** and **Shijun** for reading this thesis.

Thanks to all my friends.

I would like express my gratitude my Swedish family **Anna, Sven-Arne, Frida,** and **Jonas**, thank you family-like support, generous care and making Göteborg my second hometown. I cherish the time with you in every Eastern, Mid-summer and Christmas Eve.

My profound gratitude to my beloved parents for their love.

And most of all, **Jimmy**, for love, caring and support.

CHAPTER 8

REFERENCES

1. Dahm, R. Friedrich Miescher and the Discovery of DNA. *Dev. Biol.* **2005**, *278*, 274-288.
2. Watson, J. D.; Crick, F. H. C. Genetical Implications of the Structure of Deoxyribose Nucleic Acid. *Nature* **1953**, *171*, 964-967.
3. Lander, E. S. Initial Impact of the Sequencing of the Human Genome. *Nature* **2011**, *470*, 187-197.
4. Seeman, N. C. Nanomaterials Based on DNA. *Annu. Rev. Biochem.* **2010**, *79*, 65-87.
5. Wang, M. D.; Yin, H.; Landick, R.; Gelles, J.; Block, S. M. Stretching DNA with Optical Tweezers. *Biophys. J.* **1997**, *72*, 1335-1346.
6. Gross, P.; Laurens, N.; Oddershede, L. B.; Bockelmann, U.; Peterman, E. J. G.; Wuite, G. J. L. Quantifying How DNA Stretches, Melts and Changes Twist under Tension. *Nat. Phys.* **2011**, *7*, 731-736.
7. Van Mameren, J.; Gross, P.; Farge, G.; Hooijman, P.; Modesti, M.; Falkenberg, M.; Wuite, G. J. L.; Peterman, E. J. G. Unraveling the Structure of DNA During Overstretching by Using Multicolor, Single-Molecule Fluorescence Imaging. *Proc. Natl. Acad. Sci.* **2009**, *106*, 18231-18236.
8. Bosaeus, N.; El-Sagheer, A. H.; Brown, T.; Smith, S. B.; Åkerman, B.; Bustamante, C.; Norden, B. Tension Induces a Base-Paired Overstretched DNA Conformation. *Proc. Natl. Acad. Sci.* **2012**, *109*, 15179-15184.
9. Bosaeus, N.; El-Sagheer, A. H.; Brown, T.; Åkerman, B.; Nordén, B. Force-Induced Melting of DNA—Evidence for Peeling and Internal Melting from Force Spectra on Short Synthetic Duplex Sequences. *Nucleic Acids Res.* **2014**, *42*, 8083-8091.
10. Shokri, L.; Marintcheva, B.; Eldib, M.; Hanke, A.; Rouzina, I.; Williams, M. C. Kinetics and Thermodynamics of Salt-Dependent T7 Gene 2.5 Protein Binding to Single- and Double-Stranded DNA. *Nucleic Acids Res.* **2008**, *36*, 5668-5677.
11. Paramanathan, T.; Vladescu, I.; McCauley, M. J.; Rouzina, I.; Williams, M. C. Force Spectroscopy Reveals the DNA Structural Dynamics That Govern the Slow Binding of Actinomycin D. *Nucleic Acids Res.* **2012**, *40*, 4925-4932.

12. Reese, C. B. Oligo- and Poly-Nucleotides: 50 Years of Chemical Synthesis. *Org. Biomol. Chem.* **2005**, *3*, 3851-3868.

13. Beaucage, S. L.; Iyer, R. P. Advances in the Synthesis of Oligonucleotides by the Phosphoramidite Approach. *Tetrahedron* **1992**, *48*, 2223-2311.

14. Filippov, N. S.; Lomzov, A. A.; Pyshnyi, D. V. Thermodynamic Description of Oligonucleotide Self-Association in DNA Concatamer Structures. *Biophysics* **2009**, *54*, 280-290.

15. Shabarova, Z. A.; Dolinnaya, N. G.; Turkin, S. I.; Gromova, E. S. DNA-Like Duplexes with Repetitions. I. Properties of Concatemer Duplexes Formed by D(T-G-C-a-C-a-T-G). *Nucleic Acids Res.* **1980**, *8*, 2413-2429.

16. Simonova, O. N.; Vladimirova, A. V.; Zenkova, M. A.; Vlassov, V. V. Enhanced Cellular Binding of Concatemeric Oligonucleotide Complexes. *Biochim. Biophys. Acta, Biomembr.* **2006**, *1758*, 413-418.

17. Chen, X.; Hong, C.-Y.; Lin, Y.-H.; Chen, J.-H.; Chen, G.-N.; Yang, H.-H. Enzyme-Free and Label-Free Ultrasensitive Electrochemical Detection of Human Immunodeficiency Virus DNA in Biological Samples Based on Long-Range Self-Assembled DNA Nanostructures. *Anal. Chem.* **2012**, *84*, 8277-8283.

18. Tang, J.; Hou, L.; Tang, D.; Zhang, B.; Zhou, J.; Chen, G. Hemin/G-Quadruplex-Based Dnazyme Concatamers as Electrocatalysts and Biolabels for Amplified Electrochemical Immunosensing of Igg1. *Chem. Commun.* **2012**, *48*, 8180-8182.

19. Chen, X.; Lin, Y.-H.; Li, J.; Lin, L.-S.; Chen, G.-N.; Yang, H.-H. A Simple and Ultrasensitive Electrochemical DNA Biosensor Based on DNA Concatamers. *Chem. Commun.* **2011**, *47*, 12116-12118.

20. Ge, C.; Chen, J.; Wu, W.; Fang, Z.; Chen, L.; Liu, Q.; Wang, L.; Xing, X.; Zeng, L. An Enzyme-Free and Label-Free Assay for Copper(Ii) Ion Detection Based on Self-Assembled DNA Concatamers and Sybr Green I. *Analyst* **2013**, *138*, 4737-4740.

21. Dasgupta, D.; Goldberg, I. H. Mode of Reversible Binding of Neocarzinostatin Chromophore to DNA: Evidence for Binding Via the Minor Groove. *Biochemistry* **1985**, *24*, 6913-6920.

22. Norden, B.; Rodger, A.; Dafforn, T.; Editors *Linear Dichroism and Circular Dichroism: A Textbook on Polarized-Light Spectroscopy*; Royal Society of Chemistry Publishing, 2010

23. Larsson, C.; Rodahl, M.; Höök, F. Characterization of DNA Immobilization and Subsequent Hybridization on a 2d Arrangement of Streptavidin on a Biotin-Modified Lipid Bilayer Supported on Sio2. *Anal. Chem.* **2003**, *75*, 5080-5087.

24. Cho, Y.-K.; Kim, S.; Kim, Y. A.; Lim, H. K.; Lee, K.; Yoon, D.; Lim, G.; Pak, Y. E.; Ha, T. H.; Kim, K. Characterization of DNA Immobilization and Subsequent Hybridization Using in Situ Quartz Crystal Microbalance,

Fluorescence Spectroscopy, and Surface Plasmon Resonance. *J. Colloid Interface Sci.* **2004**, *278*, 44-52.

25. Su, X.; Wu, Y.-J.; Knoll, W. Comparison of Surface Plasmon Resonance Spectroscopy and Quartz Crystal Microbalance Techniques for Studying DNA Assembly and Hybridization. *Biosens. Bioelectron.* **2005**, *21*, 719-726.
26. Su, X.; Wu, Y.-J.; Robelek, R.; Knoll, W. Surface Plasmon Resonance Spectroscopy and Quartz Crystal Microbalance Study of Streptavidin Film Structure Effects on Biotinylated DNA Assembly and Target DNA Hybridization. *Langmuir* **2005**, *21*, 348-353.
27. Aung, K. M. M.; Ho, X.; Su, X. DNA Assembly on Streptavidin Modified Surface: A Study Using Quartz Crystal Microbalance with Dissipation or Resistance Measurements. *Sens. Actuators, B* **2008**, *B131*, 371-378.
28. Dahm, R. Discovering DNA: Friedrich Miescher and the Early Years of Nucleic Acid Research. *Hum. Genet.* **2008**, *122*, 565-581.
29. Venter, J. C.; Adams, M. D.; Myers, E. W.; Li, P. W.; Mural, R. J.; Sutton, G. G.; Smith, H. O.; Yandell, M. The Sequence of the Human Genome. *Science* **2001**, *291*, 1304-1351.
30. Crick, F. H. C. Protein Synthesis. *Symp. Soc. Exp. Biol.* **1958**, *No. 12*, 138-163.
31. Avery, O. T.; Macleod, C. M.; McCarty, M. Studis of the Chemical Nature of the Substance Inducing Transformation of Pneumococcal Types. Induction of Transformation by a Deoxyribonucleic Acid Graction Isolated from Pneumococcus Type Iii. *J. Exp. Med.* **1944**, *79*, 137-158.
32. Hershey, A. D.; Chase, M. Independent Functions of Viral Protein and Nucleic Acid in Growth of Bacteriophage. *J. Gen. Physiol.* **1952**, *36*, 39-56.
33. Kossel, A. Ueber Das Nuclein in Der Hefe. *Z. Physiol. Chem* **1879**, *3*, 284-291.
34. Kossel, A. Ueber Die Chemische Zusammensetzung Der Zelle. *DuBois-Reymond's Arch* **1891**, *181*, 181-186.
35. Levene, P. A. The Nucleic Acid of Yeast. *Biochem. Z.* **1909**, *17*, 120-131.
36. Levene, P. A.; London, E. S. Guaninedesoxypentoside from Thymus Nucleic Acid. *J. Biol. Chem.* **1929**, *81*, 711-712.
37. Levene, P. A. The Structure of Yeast Nucleic Acid. Iv. Ammonia Hydrolysis. *J. Biol. Chem.* **1919**, *40*, 415-424.
38. Franklin, R. E.; Gosling, R. G. The Structure of Sodium Thymonucleate Fibers. I. The Influence of Water Content. *Acta Crystallogr.* **1953**, *6*, 673-677.
39. Watson, J. D.; Crick, F. H. C. Molecular Structure of Nucleic Acids. A Structure for Deoxyribose Nucleic Acid. *Nature* **1953**, *171*, 737-738.
40. Chargaff, E. Chemical Specificity of Nucleic Acids and Mechanism of Their Enzymatic Degradation. *Experientia* **1950**, *6*, 201-209.
41. Franklin, R. E.; Gosling, R. G. Molecular Configuration in Sodium Thymonucleate. *Nature* **1953**, *171*, 740-741.

42. Wilkins, M. H. F.; Stokes, A. R.; Wilson, H. R. Molecular Structure of Deoxypentose Nucleic Acids. *Nature* **1953**, *171*, 738-740.

43. Mitsui, Y.; Langridge, R.; Shortle, B. E.; Cantor, C. R.; Grant, R. C.; Kodama, M.; Wells, R. D. Physical and Enzymic Studies on Poly D(I-C).Poly D(I-C), an Unusual Double-Helical DNA. *Nature* **1970**, *228*, 1166-1169.

44. Wang, A. H. J.; Quigley, G. J.; Kolpak, F. J.; Crawford, J. L.; Van, B. J. H.; Van, d. M. G.; Rich, A. Molecular Structure of a Left-Handed Double Helical DNA Fragment at Atomic Resolution. *Nature* **1979**, *282*, 680-686.

45. Spielmann, H. P.; Wemmer, D. E.; Jacobsen, J. P. Solution Structure of a DNA Complex with the Fluorescent Bis-Intercalator Toto Determined by Nmr Spectroscopy. *Biochemistry* **1995**, *34*, 8542-8553.

46. Rettig, M.; Germann, M. W.; Wang, S.; Wilson, W. D. Molecular Basis for Sequence-Dependent Induced DNA Bending. *ChemBioChem* **2013**, *14*, 323-331.

47. Kim, S. K.; Eriksson, S.; Kubista, M.; Norden, B. Interaction of 4',6-Diamidino-2-Phenylindole (Dapi) with Poly[D(G-C)2] and Poly[D(G-M5c)2]: Evidence for Major Groove Binding of a DNA Probe. *J. Am. Chem. Soc.* **1993**, *115*, 3441-3447.

48. Tabor, C. W.; Tabor, H. Polyamines. *Annu. Rev. Biochem.* **1984**, *53*, 749-790.

49. Ha, H. C.; Sirisoma, N. S.; Kuppusamy, P.; Zweier, J. L.; Woster, P. M.; Casero, R. A., Jr. The Natural Polyamine Spermine Functions Directly as a Free Radical Scavenger. *Proc. Natl. Acad. Sci.* **1998**, *95*, 11140-11145.

50. Ha, H. C.; Yager, J. D.; Woster, P. A.; Casero, R. A., Jr. Structural Specificity of Polyamines and Polyamine Analogues in the Protection of DNA from Strand Breaks Induced by Reactive Oxygen Species. *Biochem. Biophys. Res. Commun.* **1998**, *244*, 298-303.

51. Rider, J. E.; Hacker, A.; MacKintosh, C. A.; Pegg, A. E.; Woster, P. M.; Casero, R. A., Jr. Spermine and Spermidine Mediate Protection against Oxidative Damage Caused by Hydrogen Peroxide. *Amino Acids* **2007**, *33*, 231-240.

52. Oh, T. J.; Kim, I. G. Polyamines Protect against DNA Strand Breaks and Aid Cell Survival against Irradiation in Escherichia Coli. *Biotechnol. Tech.* **1998**, *12*, 755-758.

53. Warters, R. L.; Newton, G. L.; Olive, P. L.; Fahey, R. C. Radioprotection of Human Cell Nuclear DNA by Polyamines: Radiosensitivity of Chromatin Is Influenced by Tightly Bound Spermine. *Radiat. Res.* **1999**, *151*, 354-362.

54. Douki, T.; Bretonniere, Y.; Cadet, J. Protection against Radiation-Induced Degradation of DNA Bases by Polyamines. *Radiat. Res.* **2000**, *153*, 29-35.

55. Gosule, L. C.; Schellman, J. A. DNA Condensation with Polyamines. I. Spectroscopic Studies. *J. Mol. Biol.* **1978**, *121*, 311-326.

56. Chattoraj, D. K.; Gosule, L. C.; Schellman, J. A. DNA Condensation with Polyamines. Ii. Electron Microscopic Studies. *J. Mol. Biol.* **1978**, *121*, 327-337.

57. Ogawa, T.; Yu, X.; Shinohara, A.; Egelman, E. H. Similarity of the Yeast Rad51 Filament to the Bacterial Reca Filament. *Science* **1993**, *259*, 1896-1899.

58. Yu, X.; Jacobs, S. A.; West, S. C.; Ogawa, T.; Egelman, E. H. Domain Structure and Dynamics in the Helical Filaments Formed by Reca and Rad51 on DNA. *Proc. Natl. Acad. Sci.* **2001**, *98*, 8419-8424.

59. Benson, F. E.; Stasiak, A.; West, S. C. Purification and Characterization of the Human Rad51 Protein, an Analogue of E. Coli Reca. *EMBO J.* **1994**, *13*, 5764-5771.

60. Demidov, V. V.; Yavnilovich, M. V.; Belotserkovskii, B. P.; Frank-Kamenetskii, M. D.; Nielsen, P. E. Kinetics and Mechanism of Polyamide ("Peptide") Nucleic Acid Binding to Duplex DNA. *Proc. Natl. Acad. Sci.* **1995**, *92*, 2637-2641.

61. Shchepinov, M. S.; Case-Green, S. C.; Southern, E. M. Steric Factors Influencing Hybridization of Nucleic Acids to Oligonucleotide Arrays. *Nucleic Acids Res.* **1997**, *25*, 1155-1161.

62. Seeman, N. C. Nucleic Acid Junctions and Lattices. *J. Theor. Biol.* **1982**, *99*, 237-247.

63. Seeman, N. C. Macromolecular Design, Nucleic-Acid Junctions, and Crystal-Formation. *J. Biomol. Struct. Dyn.* **1985**, *3*, 11-34.

64. Wang, X.; Seeman, N. C. Assembly and Characterization of 8-Arm and 12-Arm DNA Branched Junctions. *J. Am. Chem. Soc.* **2007**, *129*, 8169-8176.

65. Liu, D.; Wang, M.; Deng, Z.; Walulu, R.; Mao, C. Tensegrity: Construction of Rigid DNA Triangles with Flexible Four-Arm DNA DNA Junctions. *J. Am. Chem. Soc.* **2004**, *126*, 2324-2325.

66. Chen, J. H.; Seeman, N. C. Synthesis from DNA of a Molecule with the Connectivity of a Cube. *Nature* **1991**, *350*, 631-633.

67. Shih, W. M.; Quispe, J. D.; Joyce, G. F. A 1.7-Kilobase Single-Stranded DNA That Folds into a Nanoscale Octahedron. *Nature* **2004**, *427*, 618-621.

68. Rothemund, P. W. K. Folding DNA to Create Nanoscale Shapes and Patterns. *Nature* **2006**, *440*, 297-302.

69. Andersen, E. S.; Dong, M.; Nielsen, M. M.; Jahn, K.; Subramani, R.; Mamdouh, W.; Golas, M. M.; Sander, B.; Stark, H.; Oliveira, C. L. P.; Pedersen, J. S.; Birkedal, V.; Besenbacher, F.; Gothelf, K. V.; Kjems, J. Self-Assembly of a Nanoscale DNA Box with a Controllable Lid. *Nature* **2009**, *459*, 73-76.

70. Douglas, S. M.; Dietz, H.; Liedl, T.; Hogberg, B.; Graf, F.; Shih, W. M. Self-Assembly of DNA into Nanoscale Three-Dimensional Shapes. *Nature* **2009**, *459*, 414-418.

71. Han, D.; Pal, S.; Nangreave, J.; Deng, Z.; Liu, Y.; Yan, H. DNA Origami with Complex Curvatures in Three-Dimensional Space. *Science* **2011**, *332*, 342-346.

72. Ma, R. I.; Kallenbach, N. R.; Sheardy, R. D.; Petrillo, M. L.; Seeman, N. C. Three-Arm Nucleic-Acid Junctions Are Flexible. *Nucleic Acids Res.* **1986**, *14*, 9745-9753.

73. Wang, Y. L.; Mueller, J. E.; Kemper, B.; Seeman, N. C. Assembly and Characterization of 5-Arm and 6-Arm DNA Branched Junctions. *Biochemistry* **1991**, *30*, 5667-5674.

74. Fu, T. J.; Seeman, N. C. DNA Double-Crossover Molecules. *Biochemistry* **1993**, *32*, 3211-3220.

75. LaBean, T. H.; Yan, H.; Kopatsch, J.; Liu, F. R.; Winfree, E.; Reif, J. H.; Seeman, N. C. Construction, Analysis, Ligation, and Self-Assembly of DNA Triple Crossover Complexes. *J. Am. Chem. Soc.* **2000**, *122*, 1848-1860.

76. Shen, Z. Y.; Yan, H.; Wang, T.; Seeman, N. C. Paranemic Crossover DNA: A Generalized Holliday Structure with Applications in Nanotechnology. *J. Am. Chem. Soc.* **2004**, *126*, 1666-1674.

77. Yan, H.; Zhang, X. P.; Shen, Z. Y.; Seeman, N. C. A Robust DNA Mechanical Device Controlled by Hybridization Topology. *Nature* **2002**, *415*, 62-65.

78. Winfree, E.; Liu, F.; Wenzler, L. A.; Seeman, N. C. Design and Self-Assembly of Two-Dimensional DNA Crystals. *Nature* **1998**, *394*, 539-544.

79. He, Y.; Chen, Y.; Liu, H.; Ribbe, A. E.; Mao, C. Self-Assembly of Hexagonal DNA Two-Dimensional (2d) Arrays. *J. Am. Chem. Soc.* **2005**, *127*, 12202-12203.

80. He, Y.; Tian, Y.; Ribbe, A. E.; Mao, C. Highly Connected Two-Dimensional Crystals of DNA Six-Point-Stars. *J. Am. Chem. Soc.* **2006**, *128*, 15978-15979.

81. Malo, J.; Mitchell, J. C.; Turberfield, A. J. A Two-Dimensional DNA Array: The Three-Layer Logpile. *J. Am. Chem. Soc.* **2009**, *131*, 13574-13575.

82. Park, S. H.; Pistol, C.; Ahn, S. J.; Reif, J. H.; Lebeck, A. R.; Dwyer, C.; LaBean, T. H. Finite-Size, Fully Addressable DNA Tile Lattices Formed by Hierarchical Assembly Procedures. *Angew. Chem., Int. Ed.* **2006**, *45*, 735-739.

83. Zheng, J.; Birktoft, J. J.; Chen, Y.; Wang, T.; Sha, R.; Constantinou, P. E.; Ginell, S. L.; Mao, C.; Seeman, N. C. From Molecular to Macroscopic Via the Rational Design of a Self-Assembled 3d DNA Crystal. *Nature* **2009**, *461*, 74-77.

84. Goodman, R. P.; Berry, R. M.; Turberfield, A. J. The Single-Step Synthesis of a DNA Tetrahedron. *Chem. Commun.* **2004**, 1372-1373.

85. Goodman, R. P.; Schaap, I. A. T.; Tardin, C. F.; Erben, C. M.; Berry, R. M.; Schmidt, C. F.; Turberfield, A. J. Rapid Chiral Assembly of Rigid DNA Building Blocks for Molecular Nanofabrication. *Science* **2005**, *310*, 1661-1665.

86. Yan, H.; LaBean, T. H.; Feng, L.; Reif, J. H. Directed Nucleation Assembly of DNA Tile Complexes for Barcode-Patterned Lattices. *Proc. Natl. Acad. Sci.* **2003**, *100*, 8103-8108.

87. Ke, Y.; Sharma, J.; Liu, M.; Jahn, K.; Liu, Y.; Yan, H. Scaffolded DNA Origami of a DNA Tetrahedron Molecular Container. *Nano Lett.* **2009**, *9*, 2445-2447.

88. Kuzuya, A.; Komiyama, M. Design and Construction of a Box-Shaped 3d-DNA Origami. *Chem. Commun.* **2009**, 4182-4184.

89. Endo, M.; Hidaka, K.; Kato, T.; Namba, K.; Sugiyama, H. DNA Prism Structures Constructed by Folding of Multiple Rectangular Arms. *J. Am. Chem. Soc.* **2009**, *131*, 15570-15571.

90. Ke, Y.; Douglas, S. M.; Liu, M.; Sharma, J.; Cheng, A.; Leung, A.; Liu, Y.; Shih, W. M.; Yan, H. Multilayer DNA Origami Packed on a Square Lattice. *J. Am. Chem. Soc.* **2009**, *131*, 15903-15908.

91. Dietz, H.; Douglas, S. M.; Shih, W. M. Folding DNA into Twisted and Curved Nanoscale Shapes. *Science* **2009**, *325*, 725-730.

92. Douglas, S. M.; Chou, J. J.; Shih, W. M. DNA-Nanotube-Induced Alignment of Membrane Proteins for Nmr Structure Determination. *Proc. Natl. Acad. Sci.* **2007**, *104*, 6644-6648.

93. Berardi, M. J.; Shih, W. M.; Harrison, S. C.; Chou, J. J. Mitochondrial Uncoupling Protein 2 Structure Determined by Nmr Molecular Fragment Searching. *Nature* **2011**, *476*, 109-113.

94. Yan, H.; Park, S. H.; Finkelstein, G.; Reif, J. H.; LaBean, T. H. DNA-Templated Self-Assembly of Protein Arrays and Highly Conductive Nanowires. *Science* **2003**, *301*, 1882-1884.

95. Williams, B. A. R.; Lund, K.; Liu, Y.; Yan, H.; Chaput, J. C. Self-Assembled Peptide Nanoarrays: An Approach to Studying Protein-Protein Interactions. *Angew. Chem., Int. Ed.* **2007**, *46*, 3051-3054.

96. Stephanopoulos, N.; Liu, M.; Tong, G. J.; Li, Z.; Liu, Y.; Yan, H.; Francis, M. B. Immobilization and One-Dimensional Arrangement of Virus Capsids with Nanoscale Precision Using DNA Origami. *Nano Lett.* **2010**, *10*, 2714-2720.

97. Aldaye, F. A.; Sleiman, H. F. Sequential Self-Assembly of a DNA Hexagon as a Template for the Organization of Gold Nanoparticles. *Angew. Chem., Int. Ed.* **2006**, *45*, 2204-2209.

98. Mao, C. D.; Sun, W. Q.; Shen, Z. Y.; Seeman, N. C. A Nanomechanical Device Based on the B-Z Transition of DNA. *Nature* **1999**, *397*, 144-146.

99. Shin, J.-S.; Pierce, N. A. A Synthetic DNA Walker for Molecular Transport. *J. Am. Chem. Soc.* **2004**, *126*, 10834-10835.

100. Garcia-Parajo, M. F.; Hernando, J.; Mosteiro, G. S.; Hoogenboom, J. P.; van, D. E. M. H. P.; van, H. N. F. Energy Transfer in Single-Molecule Photonic Wires. *ChemPhysChem* **2005**, *6*, 819-827.

101. Tinnefeld, P.; Heilemann, M.; Sauer, M. Design of Molecular Photonic Wires Based on Multistep Electronic Excitation Transfer. *ChemPhysChem* **2005**, *6*, 217-222.

102. Su, W.; Schuster, M.; Bagshaw, C. R.; Rant, U.; Burley, G. A. Site-Specific Assembly of DNA-Based Photonic Wires by Using Programmable Polyamides. *Angew. Chem., Int. Ed.* **2011**, *50*, 2712-2715.

103. Douglas, S. M.; Bachelet, I.; Church, G. M. A Logic-Gated Nanorobot for Targeted Transport of Molecular Payloads. *Science* **2012**, *335*, 831-834.

104. Jiang, Q.; Song, C.; Nangreave, J.; Liu, X.; Lin, L.; Qiu, D.; Wang, Z.-G.; Zou, G.; Liang, X.; Yan, H.; Ding, B. DNA Origami as a Carrier for Circumvention of Drug Resistance. *J. Am. Chem. Soc.* **2012**, *134*, 13396-13403.

105. Zhao, Y.-X.; Shaw, A.; Zeng, X.; Benson, E.; Nystrom, A. M.; Hogberg, B. DNA Origami Delivery System for Cancer Therapy with Tunable Release Properties. *ACS Nano* **2012**, *6*, 8684-8691.

106. Bigelow, W. C.; Pickett, D. L.; Zisman, W. A. Oleophobic Monolayers: I. Films Adsorbed from Solution in Non-Polar Liquids. *J. Colloid Sci.* **1946**, *1*, 513-538.

107. Nuzzo, R. G.; Allara, D. L. Adsorption of Bifunctional Organic Disulfides on Gold Surfaces. *J. Am. Chem. Soc.* **1983**, *105*, 4481-4483.

108. Ulman, A. Formation and Structure of Self-Assembled Monolayers. *Chem. Rev.* **1996**, *96*, 1533-1554.

109. Hickman, J. J.; Ofer, D.; Laibinis, P. E.; Whitesides, G. M.; Wrighton, M. S. Molecular Self-Assembly of Two-Terminal, Voltammetric Microsensors with Internal References. *Science* **1991**, *252*, 688-691.

110. Nilebäck, E.; Feuz, L.; Uddenberg, H.; Valiokas, R.; Svedhem, S. Characterization and Application of a Surface Modification Designed for Qcm-D Studies of Biotinylated Biomolecules. *Biosensors Bioelectron.* **2011**, *28*, 407-413.

111. Green, N. M. Avidin and Streptavidin. *Methods Enzymol.* **1990**, *184*, 51-67.

112. Diamandis, E. P.; Christopoulos, T. K. The Biotin (Strept)Avidin System - Principles and Applications in Biotechnology. *Clin. Chem.* **1991**, *37*, 625-636.

113. Freitag, S.; Le Trong, I.; Klumb, L.; Stayton, P. S.; Stenkamp, R. E. Structural Studies of the Streptavidin Binding Loop. *Protein Sci.* **1997**, *6*, 1157-1166.

114. Chaier, L.; Wolf, F. J. The Properties of Streptavidin, a Biotin-Binding Protein Produced by Streptomycetes. *Arch. Biochem. Biophys.* **1964**, *106*, 1-5.

115. Hendrickson, W. A.; Paehler, A.; Smith, J. L.; Satow, Y.; Merritt, E. A.; Phizackerley, R. P. Crystal Structure of Core Streptavidin Determined from Multiwavelength Anomalous Diffraction of Synchrotron Radiation. *Proc. Natl. Acad. Sci.* **1989**, *86*, 2190-2194.

116. El-Sagheer, A. H.; Brown, T. Click Chemistry with DNA. *Chem. Soc. Rev.* **2010**, *39*, 1388-1405.

117. Åkerman, B. Effects of Supercoiling in Electrophoretic Trapping of Circular DNA in Polyacrylamide Gels. *Biophys. J.* **1998**, *74*, 3140-3151.

118. Binnig, G.; Rohrer, H. Scanning Tunneling Microscopy. *Helv. Phys. Acta* **1982**, *55*, 726-735.

119. Binnig, G.; Quate, C. F.; Gerber, C. Atomic Force Microscope. *Phys. Rev. Lett.* **1986**, *56*, 930-933.

120. Sauerbrey, G. The Use of Quartz Oscillators for Weighing Thin Layers and for Microweighing. *Z. Phys.* **1959**, *155*, 206-222.

121. Nomura, T.; Minemura, A. Behavior of a Piezoelectric Quartz Crystal in an Aqueous the Application to the Determination of Minute Aniotint Solution and of Cyanide. *NIPPON KAGAKU KAISHI* **1980**, *1980*, 1620-1625.

122. Tsortos, A.; Papadakis, G.; Mitsakakis, K.; Melzak, K. A.; Gizeli, E. Quantitative Determination of Size and Shape of Surface-Bound DNA Using an Acoustic Wave Sensor. *Biophys. J.* **2008**, *94*, 2706-2715.

123. Reviakine, I.; Johannsmann, D.; Richter, R. P. Hearing What You Cannot See and Visualizing What You Hear: Interpreting Quartz Crystal Microbalance Data from Solvated Interfaces. *Anal. Chem.* **2011**, *83*, 8838-8848.

124. Voinova, M. V.; Rodahl, M.; Jonson, M.; Kasemo, B. Viscoelastic Acoustic Response of Layered Polymer Films at Fluid-Solid Interfaces: Continuum Mechanics Approach. *Phys. Scr.* **1999**, *59*, 391-396.

125. Wood, R. W. On a Remarkable Case of Uneven Distribution of Light in a Diffraction Grating Spectrum. *Philosophical Magazine* **1902**, *4*, 396-402.

126. Strutt, J. Note on the Remarkable Case of Diffraction Spectra Described by Prof. Wood. *Philosophical Magazine* **1907**, *14*, 60-65.

127. Otto, A. Excitation of Nonradiative Surface Plasma Waves in Silver by the Method of Frustrated Total Reflection. *Z. Phys.* **1968**, *216*, 398-410.

128. Kretschmann, E.; Raether, H. Radiative Decay of Nonradiative Surface Plasmons Excited by Light. *Z. Naturforsch. A* **1968**, *23*, 2135-2136.

129. Nylander, C.; Liedberg, B.; Lind, T. Gas Detection by Means of Surface Plasmon Resonance. *Sens. Actuators* **1982**, *3*, 79-88.

130. Liedberg, B.; Nylander, C.; Lundstroem, I. Surface Plasmon Resonance for Gas Detection and Biosensing. *Sens. Actuators* **1983**, *4*, 299-304.

131. Sipova, H.; Homola, J. Surface Plasmon Resonance Sensing of Nucleic Acids: A Review. *Anal. Chim. Acta* **2013**, *773*, 9-23.

132. Roh, S.; Chung, T.; Lee, B. Overview of the Characteristics of Micro- and Nano-Structured Surface Plasmon Resonance Sensors. *Sensors* **2011**, *11*, 1565-1588.

133. Rippe, K.; Mucke, N.; Langowski, J. Superhelix Dimensions of a 1868 Base Pair Plasmid Determined by Scanning Force Microscopy in Air and in Aqueous Solution. *Nucleic Acids Res.* **1997**, *25*, 1736-1744.

134. Reimhult, E.; Zaech, M.; Höök, F.; Kasemo, B. A Multitechnique Study of Liposome Adsorption on Au and Lipid Bilayer Formation on Sio2. *Langmuir* **2006**, *22*, 3313-3319.

135. Castronovo, M.; Radovic, S.; Grunwald, C.; Casalis, L.; Morgante, M.; Scoles, G. Control of Steric Hindrance on Restriction Enzyme Reactions with Surface-Bound DNA Nanostructures. *Nano Lett.* **2008**, *8*, 4140-4145.